Pirfenidone Modulates Macrophage Polarization and Ameliorates Radiation-induced Lung Fibrosis by Inhibiting the TGF-β1/Smad3 Pathway

hangjie ying
Zhejiang Cancer Hospital
min Fang
Zhejiang Cancer Hospital
Qing Qing Hang
Zhejiang Chinese Medical University
Ya mei Chen
Zhejiang Cancer Hospital
Xu Qian
Zhejiang cancer hospital
Ming Chen (chenming@zjcc.org.cn)
The Cancer Hospital of the University of Chinese Academy of Sciences（Zhejiang Cancer Hospital）

Research

Keywords: Ionizing radiation, Pirfenidone, Radiation-induced lung fibrosis, Macrophages, Transforming growth factor-β1

Posted Date: December 15th, 2020

DOI: https://doi.org/10.21203/rs.3.rs-125322/v1

Abstract

Background Radiation-induced lung injury (RILI) mainly contributes to the complications of thoracic radiotherapy. RILI can be divided into early-stage radiation pneumonia (RP) and late-stage radiation-induced lung fibrosis (RILF). Once RILF occurs, patients will eventually develop irreversible respiratory failure; thus, a new treatment strategy to prevent RILI is urgently needed. This study explored the therapeutic effect of pirfenidone (PFD), a Food and Drug Administration (FDA)-approved drug for idiopathic pulmonary fibrosis (IPF) treatment, and its mechanism in the treatment of RILF.

Methods A series of in vitro and in vivo assays were performed to explore the role and mechanism of PFD in the prevention and treatment of RILF.

Results Collagen deposition and fibrosis in the lung were reversed by PFD treatment, which was associated with reduced M2 macrophage infiltration and inhibition of the transforming growth factor-β1(TGF-β1) /drosophila mothers against decapentaplegic 3 (Smad3) signaling pathway. Moreover, PFD treatment decreased the radiation-induced expression of TGF-β1 and phosphorylation of Smad3 in alveolar epithelial cells (AECs) and vascular endothelial cells (VECs). Furthermore, IL-4- and IL13-induced M2 macrophage polarization was suppressed by PFD treatment in vitro, resulting in reductions in the release of arginase-1(ARG-1), chitinase 3-like 3 (YM-1) and TGF-β1. Notably, the PFD-induced inhibitory effects on M2 macrophage polarization were associated with downregulation of nuclear factor kappa-B (NF-κB) p50 activity. Additionally, PFD could significantly inhibit ionizing radiation-induced chemokine secretion in MLE-12 cells and consequently impair the migration of RAW264.7 cells. PFD could also eliminate TGF-β1 from M2 macrophages by attenuating the activation of TGF-β1/Smad3.

Conclusion PFD is a potential therapeutic agent to ameliorate fibrosis in RILF by reducing M2 macrophage infiltration and inhibiting the activation of TGF-β1/Smad3.

1. Background

Radiotherapy is a standardized treatment for thoracic tumors such as lung cancer[1], esophageal cancer [2], malignant lymphoma [3] and breast cancer [4]. Because the lung is moderately sensitive to radiation, ionizing radiation can also damage the normal lung tissue near the tumor, leading to the occurrence of radiation-induced lung injury (RILI). Clinical data show that the incidence of RILI is 5-25% after radiation therapy in patients with lung cancer, followed by those with mediastinal lymphoma (5-10%) and breast cancer (1-5%) [5]. There are two clinical manifestations of RILI: early radiation pneumonia (RP) and late radiation-induced lung fibrosis (RILF). To date, corticosteroids are mainly used to control early inflammation in the clinic, while RILF leads to progressive alveolar structural disorders and irreversible pulmonary fibrous tissue remodeling, which eventually causes respiratory failure. There is currently no effective drug available to reverse RILF [6].

Based on the induction of different cytokines, there are mainly two different types of macrophages: classically activated macrophages (CAMs or M1) and alternatively activated macrophages (AAMs or M2) [7]. M1 macrophages have been shown to prevent the development of pulmonary fibrosis, and M2 macrophages are the most prominent type of macrophage in pulmonary fibrosis [8]. Therefore, the balanced transition from M1 macrophages that promote inflammation to M2 macrophages that promote fibrosis and wound healing is one of the important reasons for the development of pulmonary fibrosis after radiation.

The alveolar-capillary barrier (ACB), which is composed of vascular endothelial cells (VECs) and alveolar epithelial cells (AECs), is very sensitive to ionizing radiation. Compromise of the barrier leads to an imbalance in the regulation of myofibroblasts, resulting in excessive extracellular matrix (ECM) deposition, which eventually leads to pulmonary fibrosis [9].

Pirfenidone (PFD) is a multipotent pyridone analog that was discovered by the MARNAC company in 1974. The antifibrotic effect of PFD was first established in a bleomycin-induced IPF animal model in 1995 [10]. Later, it was shown that PFD could inhibit fibrosis by downregulating the expression of fibrogenic growth factors and inhibit the production and release of inflammatory cytokines [11-13]. PFD can also reduce the occurrence of lipid peroxidation and oxidative stress injury [14-15]. PFD has a significant inhibitory effect on pulmonary fibrosis and fibrosis in other organs and is a broad-spectrum antifibrotic drug. A number of phase III clinical studies have shown that PFD can significantly delay the decline in forced vital capacity (FVC) in patients with IPF and significantly reduce the mortality of IPF [16-17]. Based on these data, PFD became the first drug approved by the FDA to treat IPF in 2014. The pathological and physiological process of RILF is similar to that of IPF and involves the early inflammatory reaction, lung parenchymal injury, alveolar repair and interstitial fibrosis. A previous study reported that PFD could downregulate the expression of TGF-β1 in lung tissue, leading to the inhibition of RILF progression, but the deeper mechanism has not been elucidated [18].

In the present study, we investigated the protective effects of PFD on RILF in vivo and in cultured macrophages (RAW264.7 cells and bone marrow-derived macrophages) stimulated with IL-4 and IL-13, cultured alveolar epithelial cells (MLE-12 cells) and vascular endothelial cells (PMVECs) stimulated with 12 Gy X-ray in vitro. We demonstrated that PFD could reduce the polarization of M2 macrophages by inhibiting NF-κB p50 expression and inhibiting the TGF-β1/Smad3 signaling pathway to protect against RILF. PFD was also involved in the regulation of AECs and macrophages. Thus, PFD has therapeutic potential for patients with RILF.

2. Materials And Methods

2.1 Animals and Reagents

For the animal experiments, 10- to 12-week-old inbred C57BL/6 female mice (body weight 18-20 g) were provided by Shanghai Xipuer Bikai Experimental Animal Co., Ltd. (production license: SCXK 2013-0016, China) and housed in the SPF animal breeding room of the Experimental Animal Center of Zhejiang Chinese Medical University (Hangzhou, China). The mice were housed six per cage under standard conditions and had free access to food and water. The mice were transferred in and out of the SPF animal room using dedicated sealed transfer boxes with air filtration.

2.2 Irradiation and PFD Treatment

After one week of acclimation in the room, 40 female C57BL/6 mice were randomized into 4 groups: the untreated (NT, normal saline) group, radiation alone (RT) group, PFD alone (PFD group), and radiation plus PFD (RT+PFD) group. For radiation exposure, the mice were anesthetized using sodium pentobarbital (40 mg/kg, intraperitoneally) and received a single 50-Gy dose of whole lung X-ray delivered by a small animal radiation research platform (4 Gy/min; SSD=333 mm; XStrahl, USA). For PFD (Beijing Kangdini Pharmaceutical Co., Ltd., China) administration, PFD was administered orally at a dose of 300 mg/kg/day every day based on published data [19-20].

2.3 Histology

All mice were fixed on the operating table and euthanized by femoral artery exsanguination at day 150 under sodium pentobarbital anesthesia (40 mg/kg, intraperitoneally), and all efforts were made to minimize animal suffering. The right lung tissues were stored at -80°C for qRT-PCR and western blot analysis, and the left lung tissues were fixed in 4% paraformaldehyde, dehydrated, and embedded in paraffin. Then, the lung tissues were sectioned into 4 μm slices and stained with HE. Masson's trichrome was used to evaluate fibrosis based on ten fields of view in each section. The severity of fibrosis in each histological section of the lung was assessed as the mean severity score using a semiquantitative grading system described by Ashcroft et al. [21].

After deparaffinization in xylene, hydration with graded alcohol, and antigen retrieval, the tissue sections were placed in 3% hydrogen peroxide (H_2O_2) for 10 min at room temperature to inactivate endogenous peroxidases. The slides were washed three times in PBS, blocked with 2% bovine serum albumin (BSA, cat. no. B2064, Sigma, USA) for 30 min at room temperature and incubated with primary antibodies against Collagen I (1:200, cat. no. ab34710, Abcam, UK), Collagen IV (1:200, cat. no. ab6586, Abcam, UK), CD79b (1:200, cat. no. 134147, Abcam, UK), CD68(1:200, cat. no. 31630, Abcam, UK), and CD3 (1:200, cat. no. Ab16669, Abcam, UK) at 4°C overnight. The slides were then washed with PBS and incubated with HRP-conjugated secondary antibodies (1:200, Beyotime, China) for 60 min at 37°C. The slides were then washed in PBS three times, followed by detection with Dako REALTM EnVisionTM (DAB, cat. no. PW017, Sangon Biotech, China) and counterstaining with hematoxylin.

For immunohistochemical (IHC) scoring, positive reactions were defined as those showing brown signals. Five fields were randomly selected and observed under a light microscope. The intensity was scored as follows: 0: negative; 1: weak; 2: moderate; and 3: strong. The frequency of positive cells was defined as follows: 0: less than 5%; 1:5% to 25%; 2: 26% to 50%; 3,: 51% to 75%; and 4: greater than 75%. The IHC total score was calculated as the product of the intensity and frequency scores (0 to 12). After whole section examination, the IHC score was calculated as the mean total IHC score of all fields.

2.4 Immunofluorescence（IF）staining of lung tissue

IF analysis was performed on 4 μm-thick lung sections that had been dewaxed with xylene and hydrated using sequential ethanol (100, 95, 85, and 75%) and distilled water. Antigen retrieval was performed by heating the sections in 0.1% sodium citrate buffer (pH 6.0). Then, the specimens were washed with PBS and blocked with 10% FBS to eliminate nonspecific fluorescence. Immunofluorescence staining was performed using antibodies against CD68 (1:200, cat. no. 31630, Abcam, UK) and CD163 (1:200, cat. no. 182422, Abcam, UK), and the cell preparations were incubated with DyLight 488/647-labeled secondary antibodies (1:200, cat. no. 150077/ab150115, Abcam, UK).

2.5 Quantitative reverse transcription polymerase chain reaction（qRT-PCR）

Total RNA was extracted with RNAiso Plus reagent (cat. no. 108-95-2, Takara, Japan). qRT-PCR was performed using SYBR® Premix Ex Taq II (cat. no. RR820A, Takara, Japan), after reverse transcribing 1 μg RNA with PrimeScriptTM RT Master Mix (cat. no. RR036A-2, Takara, Japan). qRT-PCR analysis of the resulting cDNA was performed in triplicate with gene-specific primers on a 7500 Fast Real-time PCR system (Applied Biosystems, Thermo Fisher Scientific, USA). The qRT-PCR reaction was carried out with the following conditions: denaturation at 94°C for 2 min, followed by 40 cycles of 94°C for 15 sec and 62°C for 40 sec. Gene expression levels were normalized to β-actin by the $2^{-\Delta\Delta Ct}$ method and were determined relative to control samples. The primers for qRT-PCR are listed in Table 1.

Table 1
Primer Sequences Used to Quantitate Gene Expression

Gene	Sequence (5’ to 3’)
TNF-α	Forward: AAGGCCGGGGTGTCCTGGAG
	Reverse: AGGCCAGGTGGGGACAGCTC
iNOS	Forward: CCCTTCCGAAGTTTCTGGCAGCAGCG
	Reverse: GGCTGTCAGAGCCTCGTGGCTTTGG
Arg-1	Forward: TCATGGAAGTGAACCCAACTCTTG
	Reverse: TCAGTCCCTGGCTTATGGTTACC
YM-1	Forward: GGATGGCTACACTGGAGAAA
	Reverse: AGAAGGGTCACTCAGGATAA
CCL2	Forward: TTAAAAACCTGGATCGGAACCAA
	Reverse: GCATTAGCTTCAGATTTACGGGT
CXCL10	Forward: AAGTGCTGCCGTCATTTTCT
	Reverse: TTCATCGTGGCAATGATCTC
CXCL16	Forward: CCTTGTCTCTTGCGTTCTTCC
	Reverse: TCCAAAGTACCCTGCGGTATC
CXCL5	Forward: TGCGTTGTGTTTGCTTAACCG
	Reverse: CTTCCACCGTAGGGCACTG
CXCL1	Forward: CTGGGATTCACCTCAAGAACATC
	Reverse: CAGGGTCAAGGCAAGCCTC
GM-CSF	Forward: GGCCTTGGAAGCATGTAGAGG
	Reverse: GGAGAACTCGTTAGAGACGACTT
β-Actin	Forward: GCATTGCTGACAGGATGCAG
	Reverse: CCTGCTTGCTGATCCACATC

2.6 Western blotting

Protein samples (40 μg) were mixed with SDS-PAGE loading buffer and boiled at 100°C for 5 min. After electrophoresis, the proteins were transferred to PVDF membranes (cat. no. IPVH00010, Millipore Biotechnology, USA). The membranes were blocked with 5% BSA for 60 min at room temperature. The

membranes were incubated with primary antibodies against ARG-1 (1:1000, cat. no. ab91279, Abcam, UK), YM-1(1:1000, cat. no. ab192029, Abcam, UK), TGF-β1 (1:1000, cat. no. ab92486, Abcam, UK), p-Smad3 (1:1000, cat. no. ab52903, Abcam, UK), Smad3 (1:1000, cat. no. ab40854, Abcam, UK), NF-κB p50 (1:1000, cat. no. Sc-8414, Santa Cruz, USA), and β-Actin (1:5000, cat. no. A2228, Sigma, USA) in 5% BSA overnight at 4°C. Afterward, membranes were washed three times with TBS containing 0.5% Tween 20 (TBST) for 10 min each time at room temperature and then incubated with secondary antibodies (1:5000, cat. no. ab150077, Abcam, UK or 1:5000, cat. no. ab150113, Abcam, UK) for 60 min at room temperature. After three additional washes with TBST, immunoreactive bands were visualized using enhanced chemiluminescent reagent (ECL, cat. no. WBKLS0500, Millipore Biotechnology, USA) and quantified by ImageJ V1.8.0 (National Institutes of Health, USA) analysis software.

2.7 Cell culture

Bone marrow cells were obtained by flushing femurs from 6- to 8-week-old mice and differentiating the cells (7 days) in Dulbecco's modified Eagle's medium (DMEM, HyClone, USA) supplemented with 30 ng/mL macrophage colony stimulating factor (M-CSF, PeproTech, USA), 10% fetal bovine serum (FBS, Gibco, USA), and antibiotics (Wonder Biotech, China).

The mouse macrophage line (RAW264.7 cells) was purchased from the Cell Bank of the Chinese Academy of Sciences (Shanghai, China). RAW264.7 cells were maintained in DMEM supplemented with 10% FBS and antibiotics. Cell cultures were maintained at 37°C in a humidified atmosphere containing 5% CO_2. The medium was changed every 3 days until the culture reached 90% confluence. For experiments, cells were suspended in culture medium at a density of 1×10^6 cells/ml. Cells at passage 3-5 were used for all experiments.

A lung epithelial cell line (MLE-12 cells) and pulmonary microvascular endothelial cells (PMVECs) were obtained from the Cell Bank of the Chinese Academy of Sciences (Shanghai, China). MLE-12 cells and PMVECs were maintained in DMEM supplemented with 10% FBS and antibiotics. Cell cultures were maintained at 37°C in a humidified atmosphere containing 5% CO_2. The medium was changed every 3 days until the culture had reached 90% confluence. For experiments, cells were suspended in culture medium at a density of 1×10^6 cells/ml. Cells at passage 3-5 were used for all experiments.

2.8 Macrophage polarization and PFD treatment

PFD was dissolved in dimethyl sulfoxide (DMSO, Sigma) and used at final concentrations of 1, 10, 100 or 1000 μg/ml.

RAW264.7 cells and bone marrow-derived macrophages (BMDMs) were cultured in DMEM supplemented with PFD for 24 h before treatment with chemokines to promote macrophage polarization. After 24 h of PFD incubation, the cells were stimulated with 10 ng/ml IL-4 (Peprotech, USA) and 10 ng/ml IL-13

(Peprotech, USA) to promote M2 polarization. After an additional 24 h, cell supernatants were collected for ELISA analysis, and the cells were washed twice with PBS and harvested in RIPA or RNAiso Plus reagent for subsequent analysis.

2.9 MLE-12 and PMVECs and PFD treatment

MLE-12 cells and PMVECs were cultured in DMEM with 10% FBS supplemented with PFD for 24 h. After 24 h of PFD incubation, fresh medium was added, and the cells were stimulated with 12 Gy X-ray for an additional 24 h. Cell supernatants were collected for ELISA analysis, and the cells were washed twice with PBS and harvested in RIPA buffer for subsequent analysis.

2.10 MTT analysis of cell viability

Cells were incubated in the presence of different concentrations of PFD. MTT (3-[4,5-dimethylthiazol-2-yl]-2,5-diphenyl tetrazolium bromide) (2 mg/ml) was added to the wells and incubated for 3 h at 37°C. The reaction product formazan was extracted with DMSO, and the absorbance was measured at 540 nm as previously described [22].

2.11 Enzyme-linked immunoabsorbent assay (ELISA)

The levels of TGF-β1 (cat. no. DY1679-05, R&D, USA), CCL2 (cat. no. DY479-05, R&D, USA) and CXCL1 (cat. no. DY453-05, R&D, USA) in the cell culture supernatant of the different treatment groups were measured by their respective ELISA kits. The optical density of each sample was measured at 450 nm using a Spectra Max 190 microplate reader.

2.12 Flow cytometry

Macrophages in the different treatment groups were digested and washed with PBS 3 times. Cell suspensions were adjusted to 10^6/ μl. Antibodies against F4/80 (cat.no. 11-480-82, eBioscience, USA) and CD206 (cat. no. 12-2061-82, eBioscience, USA) were added and incubated at room temperature for 30 min, and the cells were analyzed by flow cytometry (FACS Verse assay, BD Biosciences).

2.13 IF staining of macrophages

Macrophages were cultured in 12-well plates containing glass slides and were then washed with PBS and fixed with 4% paraformaldehyde for 30 min. After permeabilization with 0.1% Triton X-100 for 10 min, the specimens were washed with PBS and then blocked with 10% FBS to eliminate nonspecific fluorescence. Immunofluorescence staining was performed using ARG-1 (1:200, cat. no. ab91279, Abcam, UK), YM-1

(1:200, cat. no. ab192029, Abcam, UK), and CD163 (1:200, cat. no. 182422, Abcam, UK) primary antibodies, and the cell preparations were incubated with DyLight 488/647-labeled secondary antibodies (1:200, cat. no. 150077/ab150115, Abcam, UK).

2.14 Macrophage migration assay.

RAW264.7 cells were seeded into the upper chamber of a transwell insert (Corning Incorporated, NY, USA) at a density of 6×10^4 cells/well in 200 μl of serum-free medium and placed on a 24-well plate containing conditioned medium obtained from nonirradiated or irradiated MLE-12 cells. After 24 h of incubation, the cell suspension in the upper chamber was aspirated, and the upper surface of the filter was carefully cleaned with cotton buds. Cells that migrated through the polycarbonate membrane were fixed with 70% ethanol for 20 min and stained with 0.5% crystal violet for 15 min. The membrane was cut away from the chamber, and migrated cells on the lower surface of the filter were counted in six representative fields with a microscope at 200 x magnification.

2.15 Cell co-culture

MLE-12 cells were cultured in DMEM supplemented with 10% FBS, cell-free medium or 50% conditioned medium from RAW264.7 cells treated with PFD (100 μg/ml) and IL-4+IL13. After 24 h, MLE-12 cells were washed twice with PBS and harvested in sample buffer as described previously for subsequent western blot analysis.

2.16 Statistical Analysis

Unless otherwise indicated, the data are presented as the means±SD of independent experiments. The statistical significance of the differences between two groups was analyzed with Student's t-tests. The calculations were performed using Prism software for Windows (GraphPad Software).

3. Results

3.1 PFD attenuates pulmonary fibrosis induced by whole-lung radiation

The chemical structure of PFD is shown in Fig. 1A. After 50 Gy of whole lung irradiation, the skin of mice in the RT and RT+PFD groups showed obvious lesions in the irradiated area, with the color changing from black to white (Fig. 1B). The skin lesions in the RT group were more serious than those in the RT+PFD group. In the RT group, the lung tissues became consolidated and white, with increased weight, and the morphological changes and increased weight were alleviated by PFD treatment (Fig. 1C-D).

HE staining showed that the alveolar structure of the lung tissue in the NC and PFD groups was clear, with slender alveolar walls and intact capillary walls. In the RT group, the alveolar wall was severely thickened, and the alveolar cavity became obviously small, with many fibroblast aggregates, and patchy fibrosis appeared around blood vessels and the pulmonary interstitial area. After PFD treatment, the histological changes in the lung tissues were significantly alleviated compared with those of the RT group. Masson staining showed that the structure of the lung tissues in the NC and PFD groups was normal. In contrast, the alveolar wall in the RT group showed obvious destruction, with increased collagen deposition (blue area in Fig. 2A), while collagen deposition was attenuated in the RT+PFD group (Fig. 2A). Collagen I and collagen IV expression in lung tissue was examined by IHC staining and showed significantly higher expression of collagen I and collagen IV in the RT group than in the NC and PFD groups. The expression of collagen I and collagen IV in the RT+PFD group was obviously decreased (Fig. 2B).

3.2 PFD inhibits ionizing radiation-induced M2 macrophage polarization

The IHC staining results showed that in the NC and PFD groups, the expression of CD68, CD79 and CD3 was negative. However, in the RT group, CD68-positive, CD79-positive and CD3-positive immune cells were abundantly distributed in the RILF area. In the RT+PFD group, the proportion of CD68-positive immune cells decreased significantly in the lung tissue (Fig. 3A). The IF staining results showed that the immune cells in the RT group were both CD68- and CD163-positive. In the NC and PFD groups, there were no CD68- or CD163-positive cells. In the RT+PFD group, there were fewer CD68- and CD163-positive cells than in the RT group (Fig. 3B). Compared with that of the NC and PFD groups, the expression of ARG-1 and YM-1 in the RT group was upregulated, as determined by qRT-PCR. In the RT+PFD group, the expression of ARG-1 and YM-1 was downregulated. However, the expression of inducible nitric oxide synthase (iNOS) and tumor necrosis factor-α (TNF-α) in the 4 treatment groups was not significantly different (Fig. 3C). The expression of these 4 proteins was the same when analyzed by western blotting (Fig. 3D).

3.3 PFD inhibits the polarization of M2 macrophages by downregulating NF-κB p50.

After RAW264.7 cells were cocultured with BMDMs in the presence of 1000 μg/mL PFD, the proliferation of both cell types was significantly inhibited. PFD at a concentration of 100 μg/mL or less had no effect on the proliferation of either cell type (Fig. 4A). PFD at a concentration of 100 μg/mL or less was used to further explore the effect of PFD on the polarity of M2 macrophages. We stimulated macrophages with 10 ng/mL IL-4 and IL-13 for 24 h after pretreatment with 100 μg/mL PFD for 24 h. Flow cytometry was used to measure the polarization of $F4/80^+/CD206^+$ M2 macrophages induced by the different treatments. Flow cytometric analysis showed that the proportion of $F4/80^+/CD206^+$ macrophages was

increased in IL-4- and IL-13-treated macrophages but decreased after PFD treatment (Fig. 4B). qRT-PCR showed that the mRNA expression of ARG-1 and YM-1 in RAW264.7 cells and BMDMs induced by IL-4 and IL-13 was inhibited by PFD. The inhibitory effects increased with increasing concentrations of PFD (Fig. 4C). The expression of ARG-1 and YM-1 protein in RAW264.7 cells and BMDMs measured by western blotting and was also be inhibited by PFD (Fig. 4D). In addition, immunocytochemical staining indicated that PFD could significantly inhibit IL-4- and IL-13-induced ARG-1, YM-1 and CD163 expression (Fig. 4E). Furthermore, the IL-4- and IL-13-induced protein expression of NF-κB p50 in RAW264.7 cells and BMDMs was inhibited by PFD (Fig. 4F).

3.4. PFD inhibits activation of the TGF-β1/Smad3 signal pathway in vivo and in vitro.

The protein expression of TGF-β1 and p-Smad3 in lung tissues was measured by western blotting and showed that in the RT+PFD group, the RT-induced expression levels of TGF-β1 and p-Smad3 were downregulated by PFD (Fig. 5A). The cytotoxicity analysis showed that 1000 μg/mL PFD for more than 48 h significantly inhibited the proliferation of MLE-12 cells and that 100 μg/mL PFD for more than 48 h significantly inhibited the proliferation of PMVECs. Therefore, MLE-12 cells and PMVECs were stimulated with 100 μg/mL PFD for no more than 24 h for the following experiments (Fig. 5B). After MLE-12 cells and PMVECs were subjected to 12 Gy irradiation, the expression of TGF-β1 and p-Smad3 was upregulated. TGF-β1 and p-Smad3 expression in MLE-12 cells and PMVECs was downregulated after pretreatment with PFD for 24 h in vitro (Fig. 5C).

3.5. PFD is involved in the crosstalk between alveolar epithelial cells and macrophages.

The expression of granulocyte-macrophage colony stimulating factor (GM-CSF), chemokine (C-C motif) ligand 2 (CCL2), chemokine (C-X-C motif) ligand 1 protein (CXCL1), CXCL5, CXCL10, and CXCL16 in MLE-12 cells was evaluated at 24 h after irradiation with increasing doses of X-ray (Fig. 6A). The secretion of CCL2 and CXCL1 in the culture supernatant of MLE-12 cells was also measured at 24 h after irradiation (Fig. 6B), and the secretion of CCL2 and CXCL1 was inhibited by PFD treatment (Fig. 6C). In addition, the Transwell assay showed that the migration of RAW264.7 cells induced by the conditioned medium of irradiated MLE-12 cells was also inhibited by PFD treatment in vitro (Fig. 6D).

TGF-β1 expression in the culture supernatants of RAW264.7 cells was significantly elevated after induction with IL-4 and IL-13. The expression of TGF-β1 was also inhibited by PFD, and the expression was lower with increasing concentrations of PFD (Fig. 6E). The protein expression of TGF-β1 and p-Smad3 in MLE-12 cells was significantly elevated after culture with the supernatant of RAW264.7 cells stimulated with IL-4 and IL-13 for 24 h, and these effects were inhibited by PFD treatment. The expression of TGF-β1 and p-Smad3 in MLE-12 cells did not change in cell-free medium with or without IL-4 and IL-13

and PFD (Fig. 6F). Taken together, these results demonstrated that PFD inhibited not only macrophage infiltration induced by chemokines secreted by irradiated MLE-12 cells but also macrophage production of TGF-β1, which could affect the activation of TGF-β1/Smad3 in MLE-12 cells.

4. Discussion

Radiotherapy plays a very important role in the treatment of thoracic tumors. It is critical to find effective drugs to treat RP and reduce the risk of RILF. Clinically, corticosteroids are mainly used to treat RP, and early intervention is expected to lead to recovery. Although the risk of RILF can be predicted by measuring many blood biochemical indexes, such as TGF-β, interleukin 6 (IL-6), Krebs von den lungen-6 (KL-6), surfactant proteins, and interleukin-1 receptor antagonist (IL-1ra) [23], most drugs for treating RILF are still in preclinical research. There are essentially no effective treatments for RILF. In the present study, we used a mouse model of RILF to investigate the antifibrotic effect of PFD (an FDA-approved drug for the treatment of IPF). RILF is a slow progressive process that generally occurs 6-18 months after radiation in both animals and humans [24-25], and 15-20 Gy whole-lung X-ray irradiation of mice is a common method to establish an RILF mouse model [26-28]. However, in our study, the mice were irradiated with 50 Gy by a small animal radiation research platform (SARRP), which is different from other small animal irradiation systems in that it satisfies all of the following requirements: high dose rate, small beam diameter and accurate dose location based on image guidance [29]. It has been reported that SARRP can improve the overall survival rate of mice by reducing lung side effects after high-precision heart irradiation [30]. Fibrosis could be seen in the lungs of mice irradiated with 30 Gy, while overt and intense fibrosis could be seen after irradiation with 60 Gy and 90 Gy [31]. Similarly, our results showed that pulmonary fibrosis in mice was severe at 150 days after 50 Gy irradiation, while orally administered 300 mg/kg PFD significantly attenuated pulmonary inflammatory infiltration and collagen accumulation. These antifibrotic effects are consistent with the results of different animal fibrosis studies [32-33].

Using a prototypical model of RILF, we confirmed that the administration of PFD could significantly inhibit ionizing radiation-induced activation of the TGF-β1/Smad3 signaling pathway. In vitro, irradiation-induced activation of the TGF-β1/Smad3 signaling pathway was significantly inhibited by PFD at concentrations less than 100 μg/mL without cytotoxicity. This finding is consistent with a recent report that PFD has a wide range of antifibrotic effects, including the inhibition of TGF-β1/Smad3 signaling [34-35]. The increased expression of TGF-β is considered to be one of the hallmarks of RILF, and the Smad signaling pathway, which is mediated by TGF-β, plays an important role in the development of RILF [36]. TGF-β can bind to two TGF-β receptors (TβRs), TβR I and TβR II, to form the TβR complex. The activated TβR complex phosphorylates Smad2/3 and transcriptional regulatory factors, which bind to Smad4 and then regulate the expression of the fibrosis-related genes Snail, Slug, Scatter, and β-catenin, thus participating in the regulation of lung fibrosis [37-38].

A large number of animal experiments have shown that the occurrence of RILI is mainly caused by a series of pathophysiological reactions that interact with a variety of damaged cells and are regulated by a variety of cytokines [39]. In our study, the recruitment of macrophages to the lungs of thoracically irradiated mice increased significantly, and most of them were M2 macrophages, which highly expressed ARG-1 and YM-1. PFD inhibited the polarization of M2 macrophages, which was characterized by a decrease in the M2 ratio and ARG-1 and YM-1 levels in vivo and in vitro. A previous study identified the p50 subunit of NF-κB as a key regulator of M2 macrophage polarization [40-41], and the downregulation of NF-κB p50 expression may be one of the mechanisms by which PFD inhibits the polarization of M2 macrophages. Macrophages play a key role in the development of RILI because they are the first line of defense against external invasion [42]. Under the induction of different cytokines, macrophages can be divided into two types. IFN-γ can promote the expression of iNOS, which is a marker of M1 macrophages. IL-4 and IL-13 can activate the activity of ARG-1, which is a marker of M2 macrophages. M1 macrophages can express large amounts of proinflammatory cytokines, including IL-6, TNF-α, and IL-1β, and induce the secretion of chemokines, such as monocyte chemotactic protein 1(MCP-1), which promote Th1 chemotaxis-mediated immune responses. In contrast, M2 macrophages express type 2 cytokines, such as IL-4, IL-10, and IL-13, which can inhibit Th1-mediated cellular immune responses and promote Th2-mediated humoral immune responses[7]. The release of M2 cytokines has also been reported to contribute to the excessive repair of damaged tissue and accelerate fibrosis, such as that induced by parasitic infections [43], fungal infections [44], and bleomycin [45]. M2 cytokines play the same role in radiation-induced fibrosis in tissues or organs, such as the skin [46-47], intestine [48] and lung [49].

We confirmed that macrophages cultured with IL-4 and IL-13 secreted high levels of TGF-β1, while PFD could significantly inhibit the expression of TGF-β1 by M2 macrophages, which was consistent with the findings of Toda M et al [50]. AECs can activate fibroblasts through epithelial-mesenchymal transition (EMT) and then differentiate into myofibroblasts, which form characteristic fibroblast foci and secrete ECM, leading to fibrosis. It has been reported that M2 macrophages but not M1 macrophages can induce EMT in AECs, and this process is mainly regulated by the TGF-β1/Smad signaling pathway. Inhibition of TGF-β1 abrogated M2 macrophage-induced EMT in AECs [51-52]. Our current study showed that only conditioned medium from RAW264.7 cells treated with IL-4+IL-13 increased the expression of TGF-β1 and p-Smad3, and the same conditioned medium from RAW264.7 cells that had been treated with PFD (100 μg/mL) significantly suppressed TGF-β1 and p-Smad3. These findings suggested that PFD-induced inhibition of TGF-β1 secretion by M2 macrophages prevents pulmonary fibrosis by inhibiting the TGF-β1/Smad3 pathway in AECs.

Irradiated AECs can secrete a large amount of chemokines, such as CCL5, CCL2 and GM-CSF [52], which recruit inflammatory monocytes and neutrophils to the injured site. Monocytes can differentiate into macrophages, and the infiltration of macrophages into damaged tissues during tissue repair is very important because macrophages are responsible for tissue homeostasis by removing cell fragments and killing invaders [53]. Our results showed that PFD could significantly inhibit the expression of multiple chemokines induced by ionizing radiation in MLE-12 cells. It has been reported that PFD reduces

macrophage infiltration in nephrectomized rats [54] and inhibits both IL-17A- and MCP-1-induced macrophage migration in vitro [55]. We hypothesize that PFD inhibits macrophage infiltration by reducing the secretion of chemokines from irradiated MLE-12 cells. Consistent with this hypothesis, we cultured macrophages with the supernatant from irradiated MLE-12 cells in Transwells. We found that the migration of macrophages was significantly enhanced in the presence of conditioned medium from irradiated MLE-12 cells, and PFD could impair macrophage migration to irradiated MLE-12 cell supernatant.

5. Conclusions

Our findings indicated that PFD is a potential therapeutic agent to ameliorate fibrosis in RILF by reducing M2 macrophage infiltration and inhibiting the activation of TGF-β1/Smad3 signaling (Fig. 7). A pilot study confirmed that PFD is effective in ameliorating the disability associated with RILF [56]. Our cancer center is also conducting a multicenter phase II clinical trial (NCT03902509) on the treatment of RILI with PFD. We believe that PFD will be beneficial RILF patients in the near future.

6. Abbreviations

RILI	Radiation-induced lung injury
RILF	Radiation-induced lung fibrosis
PFD	Pirfenidone
FDA	Food and Drug Administration
IPF	Idiopathic pulmonary fibrosis
TGF-β1	Transforming growth factor-β1
Smad3	Drosophila mothers against decapentaplegic 3
AECs	Alveolar epithelial cells
VECs	Vascular endothelial cells
ARG-1	Arginase-1
YM-1	Chitinase 3-like 3
NF-κB	Nuclear factor kappa-B
RP	Radiation pneumonia
CAMs	Alassically activated macrophages
AAMs	Alternatively activated macrophages
ACB	Alveolar-capillary barrier
ECM	Extracellular matrix
FVC	Forced vital capacity
IHC	Immunohistochemical
IF	Immunofluorescence
DMEM	Dulbecco's modified Eagle's medium
MCSF	Macrophage colony stimulating factor
FBS	Fetal bovine serum
PMECs	Pulmonary microvascular endothelial cells
qRT-PCR	Quantitative real-time polymerase chain reaction
DMSO	Dimethyl sulfoxide
BMDM	Bone marrow-derived macrophages
CCL2	(C-C motif) ligand 2
CXCL1	chemokine (C-X-C motif) ligand 1

IL-6	Interleukin 6
KL-6	Krebs von den lungen-6
iNOS	Inducible nitric oxide synthase
IL-1ra	Interleukin-1 receptor antagonist
TNF-α	Tumor necrosis factor-α
GM-CSF	Granulocyte-macrophage colony stimulating factor
SARRP	Small animal radiation research platform
TβRs	TGF-β receptors
MCP-1	Monocyte chemotactic protein 1
ELISA	Enzyme-linked immunoabsorbent assay
EMT	**Epithelial-mesenchymal transition**

7. Declarations

7.1 Ethics approval and consent to participate

Animal experiments were implemented following the ethical standards of animal experiment ratified by Animal Management Committee in Zhejiang Cancer Hospital.

7.2 Consent for publication

Not applicable

7.3 Availability of data and material

Not applicable

7.4 Competing interests

The authors declare no conflict of interest.

7.5 Funding

This work was supported by the National Natural Science Foundation of China (No.81703018), Natural Science Foundation of Zhejiang Province (No. LY21H160004), and Medical Health Science and

Technology Project of Zhejiang Provincial Health Commission (No.2020KY466, No.2021KY084).

7.6 Authors' contribution

FM and YHJ performed the statistical analyses and wrote the manuscript. YHJ, HQQ and CYM participated in experiment preparation and performed the experiments. CM contributed to the study design, CM and QX contributed to revise critically the manuscript. All the authors read and approved the final version of the manuscript.

7.7 Acknowledgements

We give our sincere gratitude to the reviewers for their valuable suggestions.

References

1. Baker S, Dahele M, Lagerwaard FJ, Senan S. A critical review of recent developments in radiotherapy for non-small cell lung cancer. Radiat Oncol. 2016;11:115.
2. Zhang M, Wu AJ. Radiation techniques for esophageal cancer.Chin Clin Oncol. 2017; 6:45.
3. Urwin R, Barrington SF, Mikhaeel NG. Role of PET imaging in adaptive radiotherapy for lymphoma. Q J Nucl Med Mol Imaging 2018; 62:411-9.
4. Castaneda SA, Strasser J.Updates in the Treatment of Breast Cancer with Radiotherapy.Surg Oncol Clin N Am. 2017; 26:371-82.
5. Yavas G, Calik M, Calik G, Yavas C, Ata O, Esme H. The effect of Halofuginone in the amelioration of radiation induced-lung fibrosis. Med Hypotheses. 2013; 80:357-9.
6. Rajan Radha R, Chandrasekharan G. Pulmonary injury associated with radiation therapy-Assessment, complications and therapeutic targets. Biomed Pharmacother. 2017; 89: 1092-104.
7. Ying H, Kang Y, Zhang H, Zhao D, Xia J, Lu Z, et al. MiR-127 modulates macrophage polarization and promotes lung inflammation and injury by activating the JNK pathway. J Immunol. 2015;194:1239-51.
8. Zhang H, Han G, Liu H, Chen J, Ji X, Zhou F, et al.The development of classically and alternatively activated macrophages has different effects on the varied stages of radiation-induced pulmonary injury in mice. J Radiat Res. 2011; 52:717-26.
9. Huang Y, Zhang W, Yu F, Gao F. The Cellular and Molecular Mechanism of Radiation-Induced Lung Injury. Med Sci Monit. 2017; 23: 3446-50.
10. Iyer SN, Wild JS, Schiedt MJ, Hyde DM, Margolin SB, Giri SN. Dietary intake of pirfenidone ameliorates bleomycin-induced lung fibrosis in hamsters. J Lab Clin Med. 1995;125:779-85.
11. Sun YW, Zhang YY, Ke XJ, Wu XJ, Chen ZF, Chi P. Pirfenidone prevents radiation-induced intestinal fibrosis in rats by inhibiting fibroblast proliferation and differentiation and suppressing the TGF-

β1/Smad/CTGF signaling pathway. Eur J Pharmacol. 2018; 822:199-206.

12. Cui Y, Zhang M, Leng C, Blokzijl T, Jansen BH, Dijkstra G, et al. Pirfenidone Inhibits Cell Proliferation and Collagen I Production of Primary Human Intestinal Fibroblasts. Cells. 2020; 9:775.
13. Jin J, Togo S, Kadoya K, Tulafu M, Namba Y, Iwai M, et al. Pirfenidone attenuates lung fibrotic fibroblast responses to transforming growth factor-β1. Respir Res. 2019; 20: 119.
14. Pourgholamhossein F, Rasooli R, Pournamdari M, Pourgholi L, Samareh-Fekri M, Ghazi-Khansari M, et al. Pirfenidone protects against paraquat-induced lung injury and fibrosis in mice by modulation of inflammation, oxidative stress, and gene expression. Food Chem Toxicol. 2018;112:39-46.
15. Rasooli R, Pourgholamhosein F, Kamali Y, Nabipour F, Mandegary A. Combination Therapy with Pirfenidone plus Prednisolone Ameliorates Paraquat-Induced Pulmonary Fibrosis. Inflammation. 2018; 41:134-42.
16. Noble PW, Albera C, Bradford WZ, Costabel U, Glassberg MK, Kardatzke D, et al. Pirfenidone in patients with idiopathic pulmonary fibrosis(CAPACITY):two randomised trials. Lancet. 2011; 377:1760-9.
17. King TE Jr, Bradford WZ, Castro-Bernardini S, Fagan EA, Glaspole I, Glassberg MK, et al. A Phase 3 Trial of Pirfenidone in patients with Idiopathic Pulmonary Fibrosis. N ENGL J MED. 2014; 370: 2083-91.
18. Qin W, Liu B, Yi M, Li L, Tang Y, Wu B, et al. Antifibrotic Agent Pirfenidone Protects against Development of Radiation-Induced Pulmonary Fibrosis in a Murine Model. Radiat Res. 2018; 190:396-403.
19. Li G, Ren J, Hu Q, Deng Y, Chen G, Guo K, et al. Oral pirfenidone protects against fibrosis by inhibiting fibroblast proliferation and TGF-β signaling in a murine colitis model. Biochem Pharmacol. 2016;117: 57-67.
20. Sandoval-Rodriguez A, Monroy-Ramirez HC, Meza-Rios A, Garcia-Bañuelos J, Vera-Cruz J, Gutiérrez-Cuevas J,et al. Pirfenidone Is an Agonistic Ligand for PPARα and Improves NASH by Activation of SIRT1/LKB1/pAMPK. Hepatol Commun. 2020;4:434-49.
21. Ashcroft T, Simpson JM, Timbrell V. Simple method of estimating severity of pulmonary fibrosis on a numerical scale. J Clin Pathol.1988; 41: 467-70.
22. Mota A, Jiménez-Garcia L, Herránz S, de Las Heras B, Hortelano S. α-Hispanolol sensitizes hepatocellular carcinoma cells to TRAIL-induced apoptosis via death receptor up-regulation. Toxicol Appl Pharmacol. 2015; 286:168-77.
23. Kong FM, Ao X, Wang L, Lawrence TS.The use of blood biomarkers to predict radiation lung toxicity: a potential strategy to individualize thoracic radiation therapy. Cancer Control. 2008; 15:140-50.
24. Travis EL, Tucker SL. The relationship between functional assays of radiation response in the lung and target cell depletion. Br J Cancer Suppl. 1986;7:304-19.
25. Siemann DW, Hill RP, Penney DP. Early and late pulmonary toxicity in mice evaluated 180 and 420 days following localized lung irradiation. Radiat Res. 1982; 89: 396-407.

26. Li X, Xu G, Qiao T, Yuan S, Zhuang X, Zhang J, et al. Effects of CpG Oligodeoxynucleotide 1826 on transforming growth factor-beta 1 and radiation-induced pulmonary fibrosis in mice. J Inflamm (Lond). 2016;13:16.
27. Zhang C, Zhao H, Li BL, Fu Gao, Liu H, Cai JM, et al. CpG-oligodeoxynucleotides may be effective for preventing ionizing radiation induced pulmonary fibrosis. Toxicol Lett. 2018; 292:181-9.
28. Bickelhaupt S, Erbel C, Timke C, Wirkner U, Dadrich M, Flechsig P, et al. Effects of CTGF Blockade on Attenuation and Reversal of Radiation-Induced Pulmonary Fibrosis. J Natl Cancer Inst. 2017;109(8).
29. Cho J, Kodym R, Seliounine S, Richardson JA, Solberg TD, Story MD. High dose-per-fraction irradiation of limited lung volumes using an image-guided, highly focused irradiator: simulating stereotactic body radiotherapy regimens in a small-animal model. Int J Radiat Oncol Biol Phys. 2010;77:895-902.
30. Sievert W, Stangl S, Steiger K, Multhoff G. Improved Overall Survival of Mice by Reducing Lung Side Effects After High-Precision Heart Irradiation Using a Small Animal Radiation Research Platform. Int J Radiat Oncol Biol Phys. 2018 ;101:671-9.
31. Hong ZY, Lee CG, Shim HS, Lee EJ, Song KH, Choi BW, et al. Time, Dose, and Volume Responses in a Mouse Pulmonary Injury Model Following Ablative Irradiation. Lung. 2016 ;194:81-90.
32. Li Y, Li H, Liu S, Pan P, Su X, Tan H, et al. Pirfenidone ameliorates lipopolysaccharide-induced pulmonary inflammation and fibrosis by blocking NLRP3 inflammasome activation. Mol Immunol. 2018; 99:134-44.
33. Li G, Ren J, Hu Q, Deng Y, Chen G, Guo K, et al. Oral pirfenidone protects against fibrosis by inhibiting fibroblast proliferation and TGF-β signaling in a murine colitis model. Biochem Pharmacol. 2016;117:57-67.
34. Ma Z, Zhao C, Chen Q, Yu C, Zhang H, Zhang Z, et al. Antifibrotic effects of a novel pirfenidone derivative in vitro and in vivo. Pulm Pharmacol Ther. 2018 ;53:100-6.
35. Conte E, Gili E, Fagone E, Fruciano M, Iemmolo M, Vancheri C. Effect of pirfenidone on proliferation, TGF-β-induced myofibroblast differentiation and fibrogenic activity of primary human lung fibroblasts. Eur J Pharm Sci. 2014;58:13-9.
36. Chen Z, Wu Z, Ning W. Advances in Molecular Mechanisms and Treatment of Radiation-Induced Pulmonary Fibrosis. Transl Oncol. 2019; 12:162-9.
37. Kalluri R, Neilson EG. Epithelial-mesenchymal transition and its implications for fibrosis. J Clin Invest. 2003; 112: 1776-84.
38. Derynck R, Zhang YE. Smad-dependent and Smad-independent pathways in TGF-beta family signalling. Nature. 2003; 425: 577-84.
39. Lu L, Sun C, Su Q, Wang Y, Li J, Guo Z,et al. Radiation-induced lung injury: latest molecular developments, therapeutic approaches, and clinical guidance. Clin Exp Med. 2019;19: 417-26.
40. Porta C. Porta, M. Rimoldi, G. Raes, L. Brys, P. Ghezzi, D. et al., Tolerance and M2 (alternative) macrophage polarization are related processes orchestrated by p50 nuclear factor kappaB. Proc. Natl. Acad. Sci. U.S.A. 2009;106:14978-83.

41. Lu H, Wu L, Liu L, Ruan Q, Zhang X, Hong W, et al. Quercetin ameliorates kidney injury and fibrosis by modulating M1/M2 macrophage polarization. Biochem Pharmacol. 2018 ;154: 203-12.
42. Murthy S, Larson-Casey JL, Ryan AJ, He C, Kobzik L, Carter AB. Alternative activation of macrophages and pulmonary fibrosis are modulated by scavenger receptor, macrophage receptor with collagenous structure. FASEB J. 2015; 29: 3527-36
43. Chiaramonte MG, Mentink-Kane M, Jacobson BA, Cheever AW, Whitters MJ, Goad ME,et al. Regulation and function of the interleukin 13 receptor alpha 2 during a T helper cell type 2-dominant immune response. J Exp Med. 2003; 197: 687-701.
44. Blease K, Jakubzick C, Schuh JM, Joshi BH, Puri RK, Hogaboam CM. IL-13 fusion cytotoxin ameliorates chronic fungal-induced allergic airway disease in mice. J Immunol. 2001; 167: 6583-592.
45. Jakubzick C, Choi ES, Joshi BH, Keane MP, Kunkel SL, Puri RK,et al.Therapeutic attenuation of pulmonary fibrosis via targeting of IL-4- and IL-13-responsive cells. J Immunol. 2003; 171: 2684-93.
46. Horton JA, Hudak KE, Chung EJ, White AO, Scroggins BT, Burkeen JF,et al. Mesenchymal stem cells inhibit cutaneous radiation-induced fibrosis by suppressing chronic inflammation. Stem Cell. 2013; 31: 2231-41.
47. Riccobono D, Nikovics K, François S, Favier AL, Jullien N, Schrock G,et al. First Insights Into the M2 Inflammatory Response After Adipose-Tissue-Derived Stem Cell Injections in Radiation-Injured Muscles. Health Phys. 2018; 115: 37-48.
48. Rannou E, François A, Toullec A, Guipaud O, Buard V, Tarlet G,et al. In vivo evidence for an endothelium-dependent mechanism in radiation-induced normal tissue injury. Sci Rep. 2015; 5: 15738.
49. Duru N, Wolfson B, Zhou Q. Mechanisms of the alternative activation of macrophages and non-coding RNAs in the development of radiation-induced lung fibrosis. World J Biol Chem. 2016; 7: 231-9.
50. Toda M, Mizuguchi S, Minamiyama Y, Yamamoto-Oka H, Aota T, Kubo S, et al. Pirfenidone suppresses polarization to M2 phenotype macrophages and the fibrogenic activity of rat lung fibroblasts. J Clin Biochem Nutr. 2018; 63: 58-65.
51. Zhu L, Fu X, Chen X, Han X, Dong P. M2 macrophages induce EMT through the TGF-β/Smad2 signaling pathway. Cell Biol Int. 2017; 41:960-8.
52. Park HR, Jo SK, Jung U. Ionizing Radiation Promotes Epithelial-to-Mesenchymal Transition in Lung Epithelial Cells by TGF-β-producing M2 Macrophages. In Vivo. 2019;33:1773-84.
53. Cao Z, Lis R, Ginsberg M, Chavez D, Shido K, Rabbany SY, et al.Targeting of the pulmonary capillary vascular niche promotes lung alveolar repair and ameliorates fibrosis. Nat Med. 2016; 22: 154-62.
54. Chen JF, Ni HF, Pan MM, Liu H, Xu M, Zhang MH, et al. Pirfenidone inhibits macrophage infiltration in 5/6 nephrectomized rats. Am J Physiol Renal Physiol. 2013; 304:676-85.
55. Du J, Paz K, Flynn R, Vulic A, Robinson TM, Lineburg KE, et al. Pirfenidone ameliorates murine chronic GVHD through inhibition of macrophage infiltration and TGF-β production. Blood. 2017;129:2570-80.

56. Simone NL, Soule BP, Gerber L, Augustine E, Smith S, Altemus RM, et al. Oral pirfenidone in patients with chronic fibrosis resulting from radiotherapy: a pilot study. Radiat Oncol. 2007, 31; 2:19.

Figures

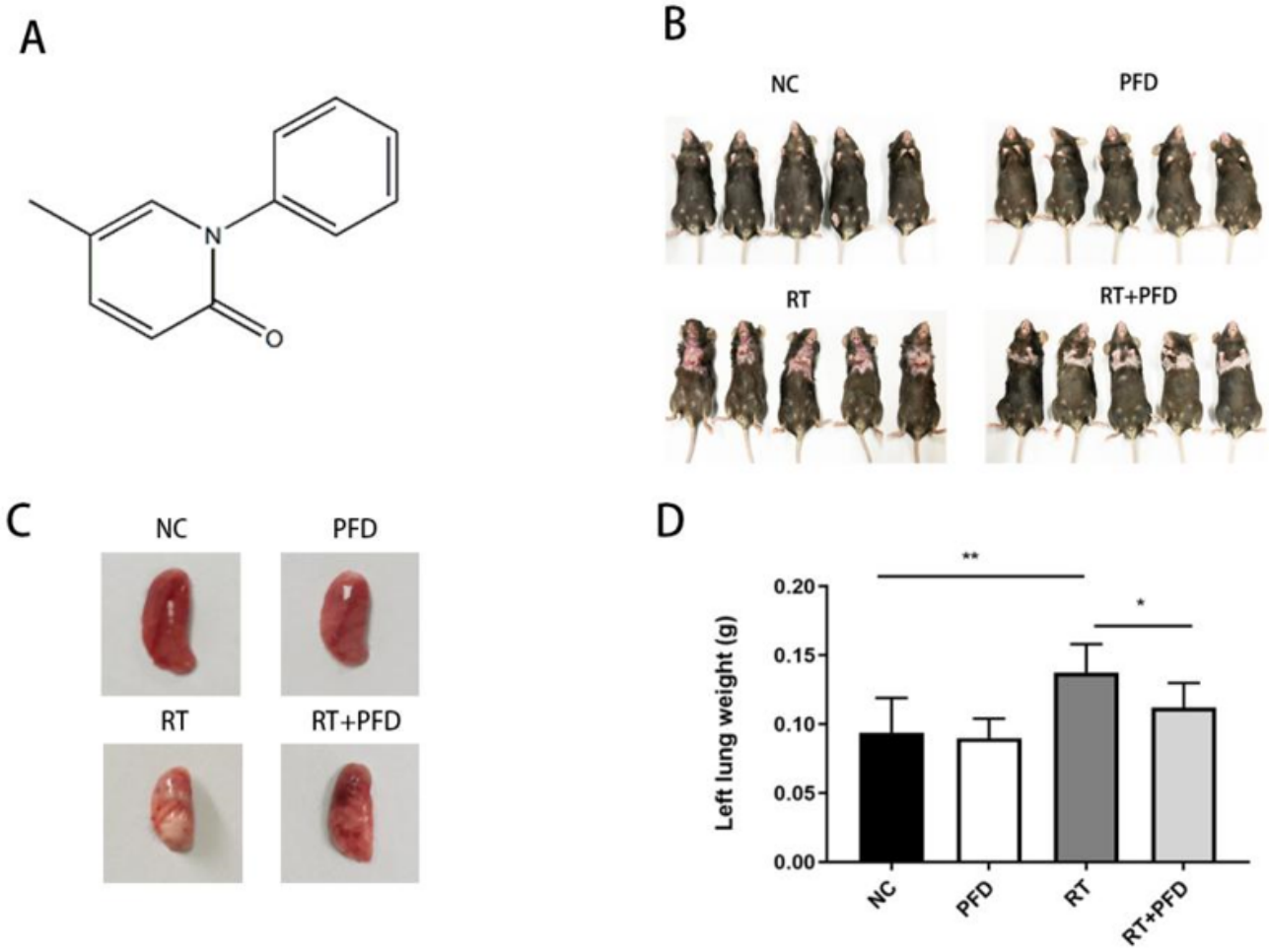

Figure 1

PFD attenuated pulmonary fibrosis induced by whole lung irradiation (A). Chemical structure of PFD. (B). Photographs of mice in the 4 groups after 84 days of treatment. (C). Photographs of the lung tissue in the 4 groups. (D). The mean left lung weights of mice in the 4 groups. The values are the means ±SD, *p<0.05, **p<0.01.

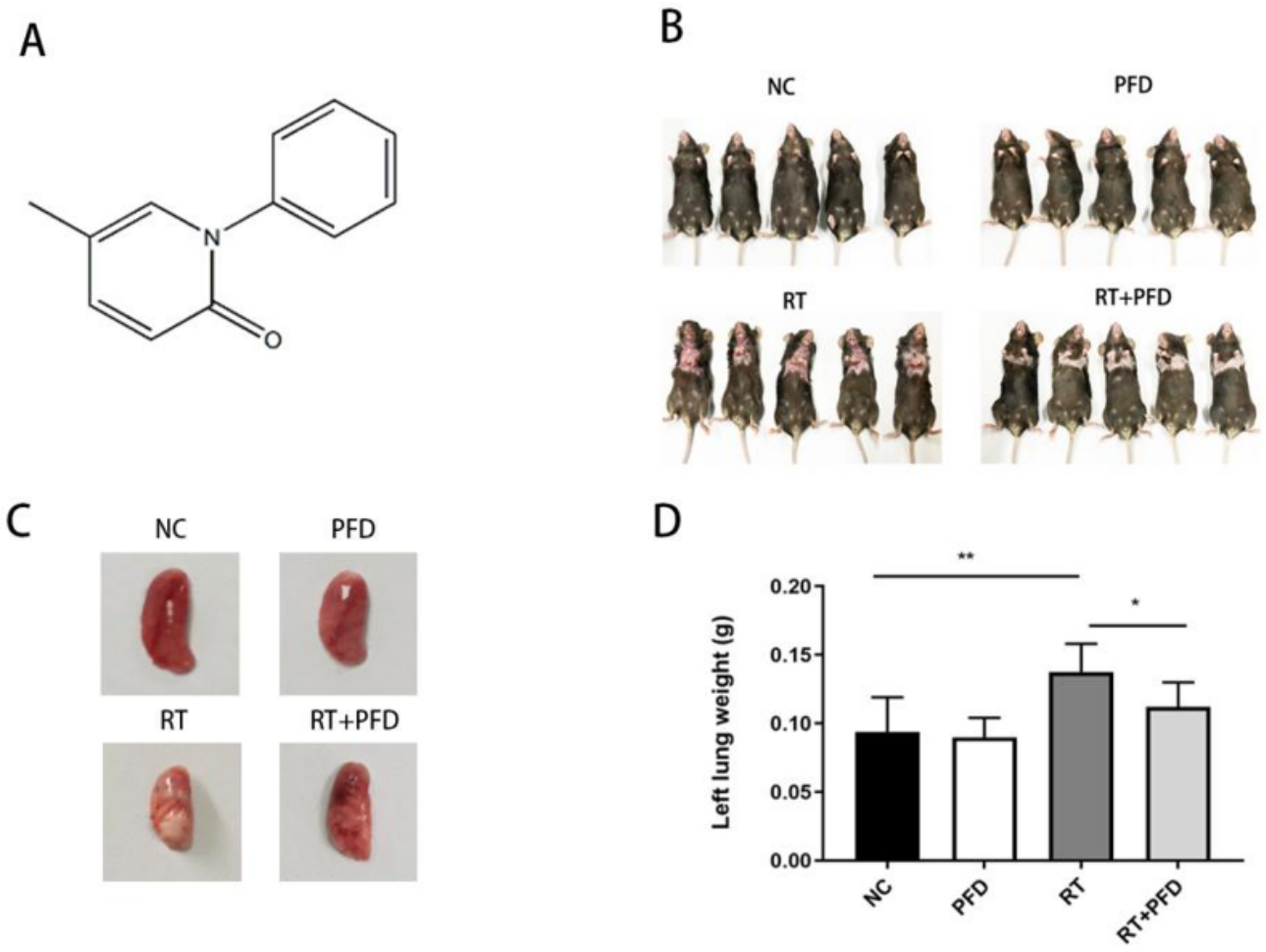

Figure 1

PFD attenuated pulmonary fibrosis induced by whole lung irradiation (A). Chemical structure of PFD. (B). Photographs of mice in the 4 groups after 84 days of treatment. (C). Photographs of the lung tissue in the 4 groups. (D). The mean left lung weights of mice in the 4 groups. The values are the means ±SD, *p<0.05, **p<0.01.

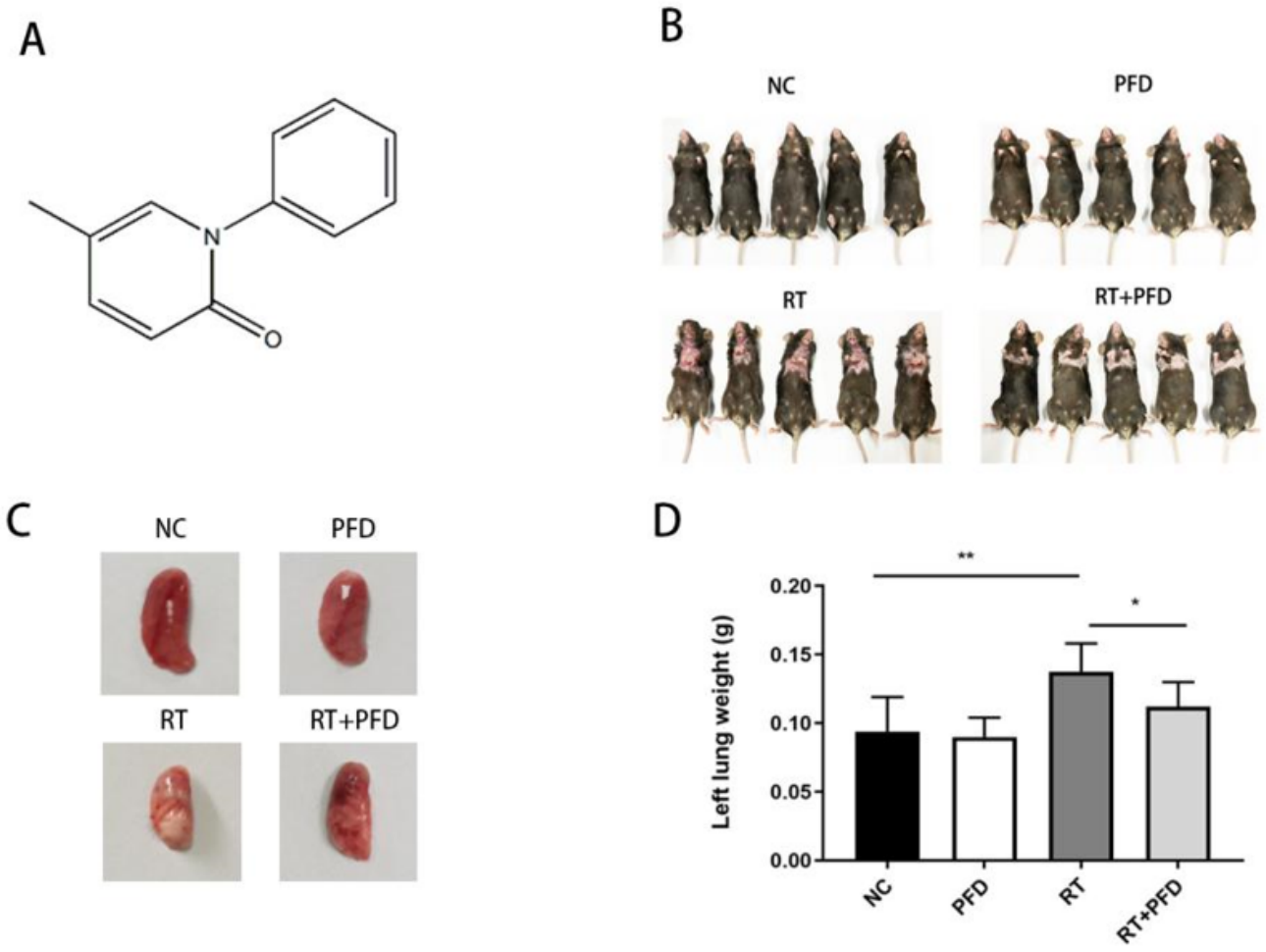

Figure 1

PFD attenuated pulmonary fibrosis induced by whole lung irradiation (A). Chemical structure of PFD. (B). Photographs of mice in the 4 groups after 84 days of treatment. (C). Photographs of the lung tissue in the 4 groups. (D). The mean left lung weights of mice in the 4 groups. The values are the means ±SD, *p<0.05, **p<0.01.

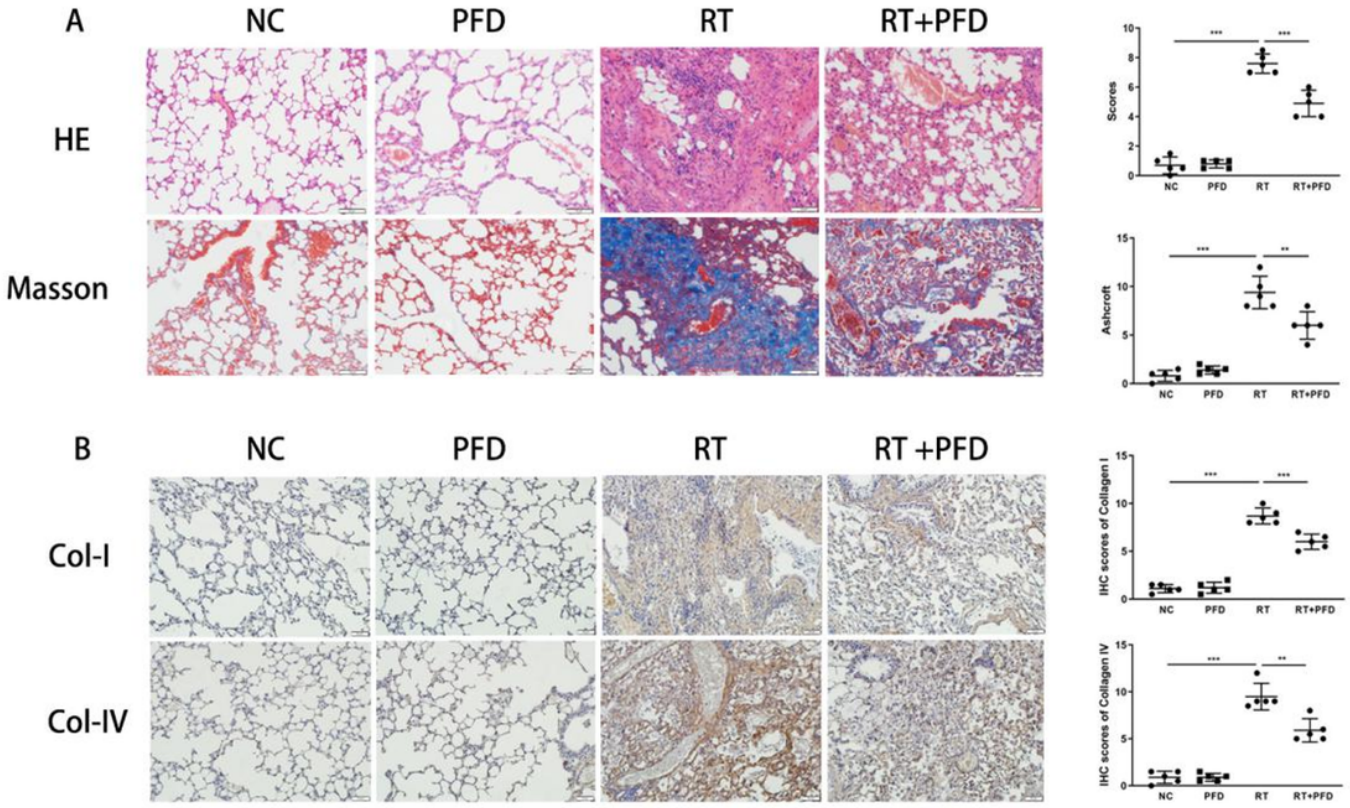

Figure 2

PFD effectively inhibited alveolar inflammation, pulmonary fibrosis and collagen deposition induced by lung irradiation. (A). PFD effectively inhibited alveolar inflammation, pulmonary fibrosis and collagen deposition induced by lung irradiation. (A) HE and Masson staining of lung tissues in the 4 groups and semiquantitative analysis of the degree of pulmonary fibrosis. (B) IHC staining of collagen I and collagen IV in lung tissue from the 4 groups and semiquantitative analysis of collagen I and collagen IV expression. Scale bar = 50 μm. The values are the means ±SD, **p<0.01, ***p<0.001.

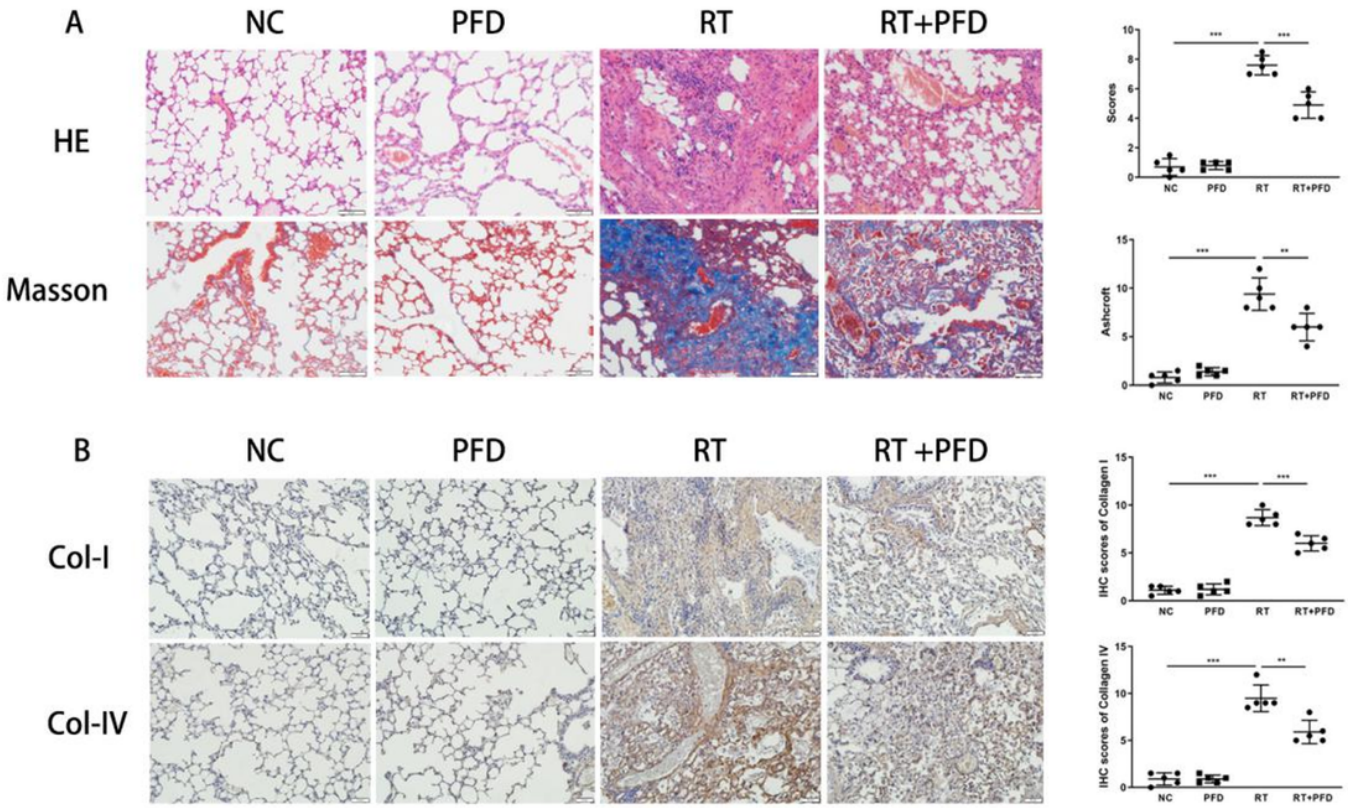

Figure 2

PFD effectively inhibited alveolar inflammation, pulmonary fibrosis and collagen deposition induced by lung irradiation. (A). PFD effectively inhibited alveolar inflammation, pulmonary fibrosis and collagen deposition induced by lung irradiation. (A) HE and Masson staining of lung tissues in the 4 groups and semiquantitative analysis of the degree of pulmonary fibrosis. (B) IHC staining of collagen I and collagen IV in lung tissue from the 4 groups and semiquantitative analysis of collagen I and collagen IV expression. Scale bar = 50 μm. The values are the means ±SD, **p<0.01, ***p<0.001.

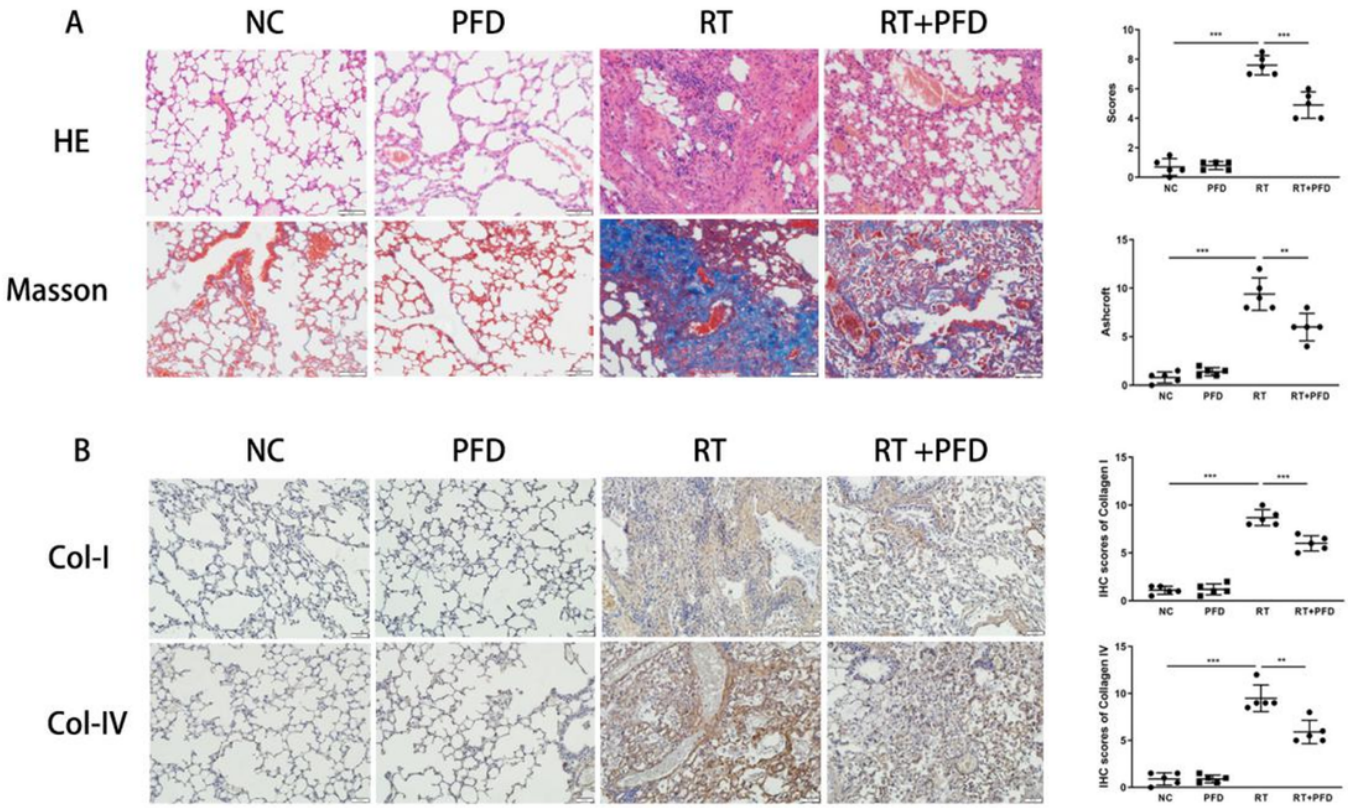

Figure 2

PFD effectively inhibited alveolar inflammation, pulmonary fibrosis and collagen deposition induced by lung irradiation. (A). PFD effectively inhibited alveolar inflammation, pulmonary fibrosis and collagen deposition induced by lung irradiation. (A) HE and Masson staining of lung tissues in the 4 groups and semiquantitative analysis of the degree of pulmonary fibrosis. (B) IHC staining of collagen I and collagen IV in lung tissue from the 4 groups and semiquantitative analysis of collagen I and collagen IV expression. Scale bar = 50 μm. The values are the means ±SD, **p<0.01, ***p<0.001.

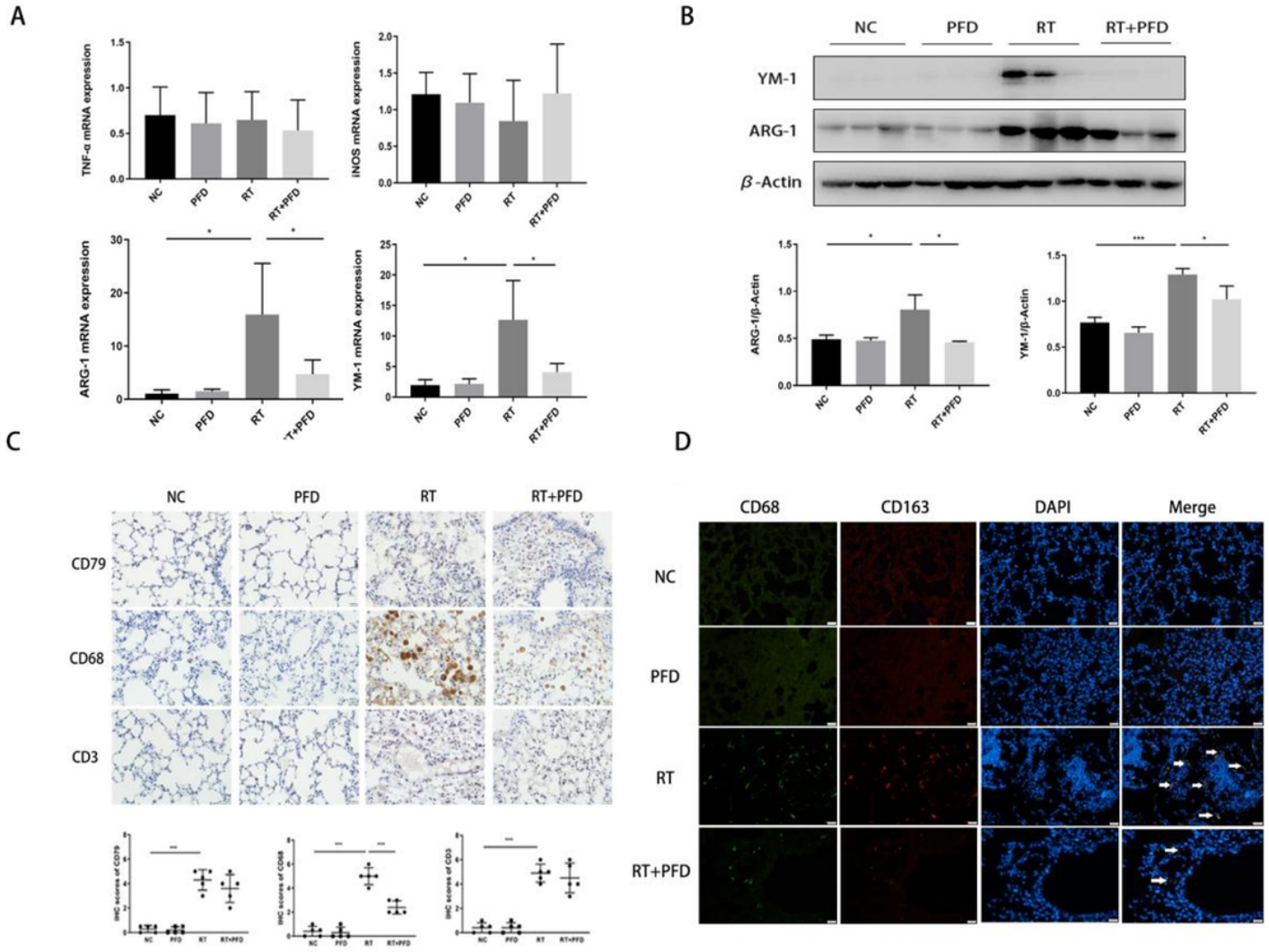

Figure 3

PFD inhibits ionizing radiation-induced M2 polarization. (A). The expression of CD68, CD79 and CD3 in the lung tissue of mice in the different treatment groups was determined by IHC analysis (B). Lung sections were fixed and stained with anti-CD68 (green) and anti-CD163 (red). Arrows point to cells that are CD68+CD163+. Scale bar = 20 μm. (C). qRT-PCR was used to measure the expression of ARG-1, YM-1, iNOS and TNF-α in the lung tissue of mice in the different treatment groups. (D). Western blotting was used to measure the expression of ARG-1 and YM-1 in the lung tissue of mice in the different treatment groups. The values are the means ±SD, *p<0.05, **p<0.01,***p<0.001.

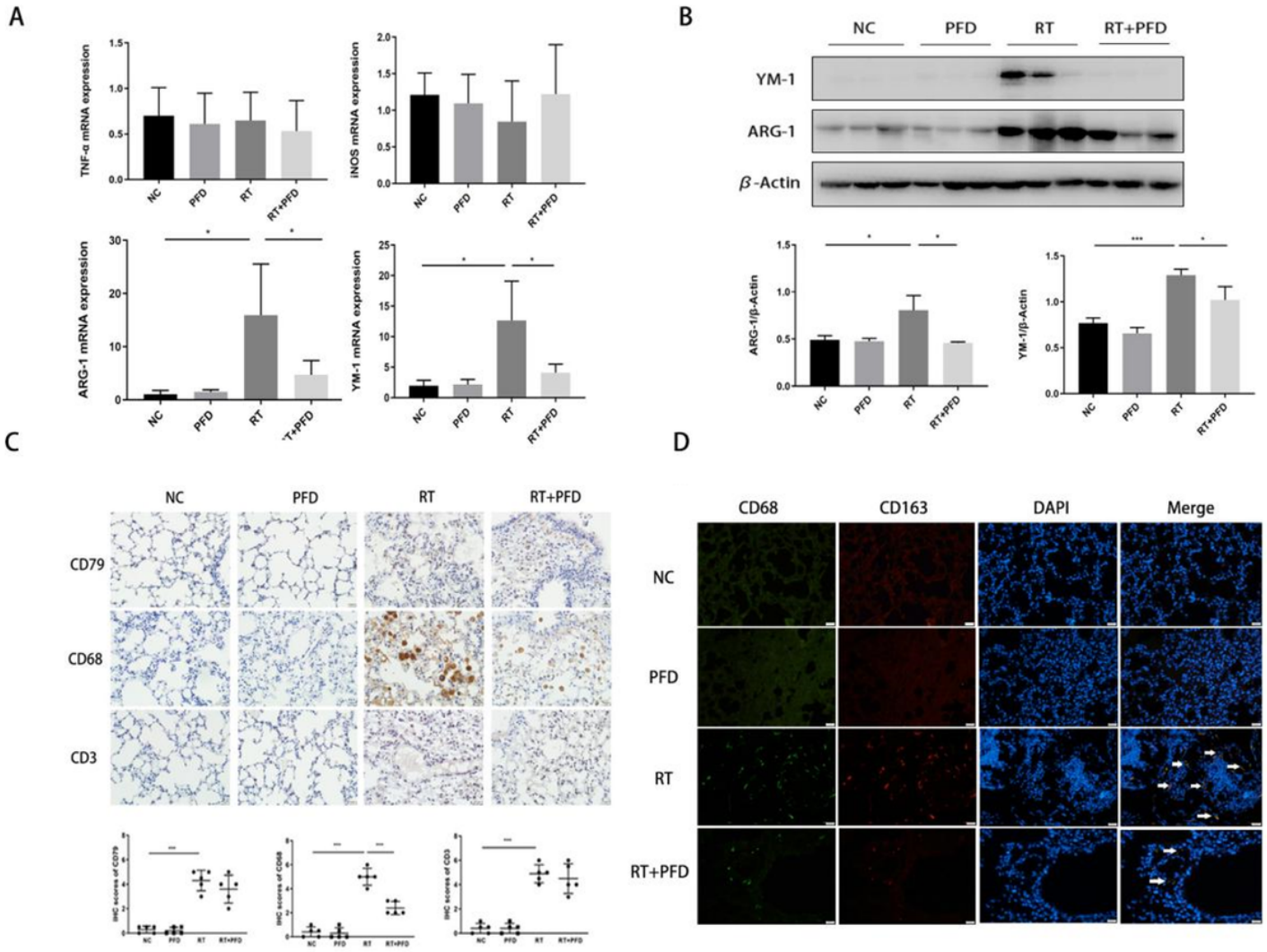

Figure 3

PFD inhibits ionizing radiation-induced M2 polarization. (A). The expression of CD68, CD79 and CD3 in the lung tissue of mice in the different treatment groups was determined by IHC analysis (B). Lung sections were fixed and stained with anti-CD68 (green) and anti-CD163 (red). Arrows point to cells that are CD68+CD163+. Scale bar = 20 μm. (C). qRT-PCR was used to measure the expression of ARG-1, YM-1, iNOS and TNF-α in the lung tissue of mice in the different treatment groups. (D). Western blotting was used to measure the expression of ARG-1 and YM-1 in the lung tissue of mice in the different treatment groups. The values are the means ±SD, *p<0.05, **p<0.01,***p<0.001.

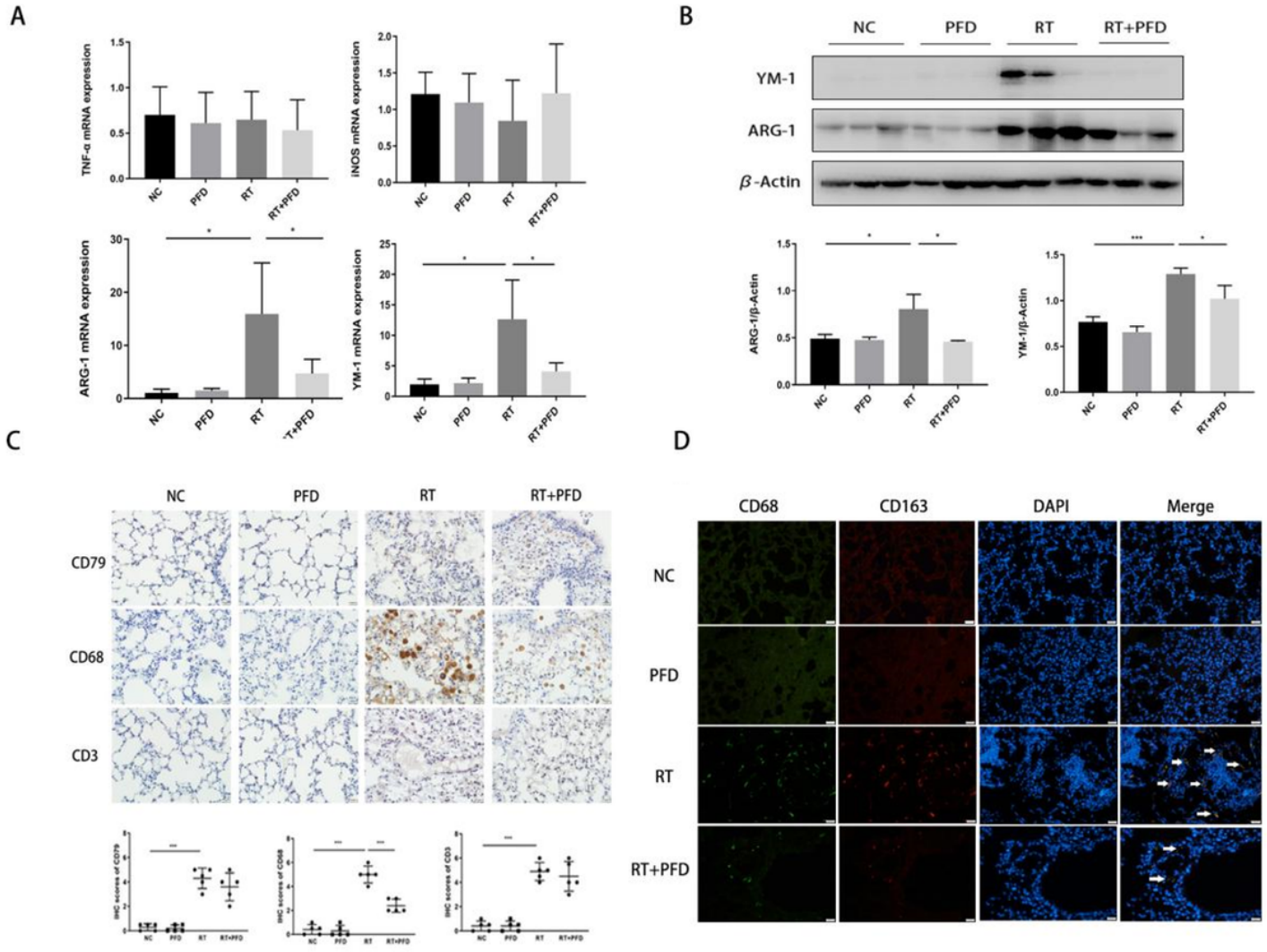

Figure 3

PFD inhibits ionizing radiation-induced M2 polarization. (A). The expression of CD68, CD79 and CD3 in the lung tissue of mice in the different treatment groups was determined by IHC analysis (B). Lung sections were fixed and stained with anti-CD68 (green) and anti-CD163 (red). Arrows point to cells that are CD68+CD163+. Scale bar = 20 μm. (C). qRT-PCR was used to measure the expression of ARG-1, YM-1, iNOS and TNF-α in the lung tissue of mice in the different treatment groups. (D). Western blotting was used to measure the expression of ARG-1 and YM-1 in the lung tissue of mice in the different treatment groups. The values are the means ±SD, *p<0.05, **p<0.01,***p<0.001.

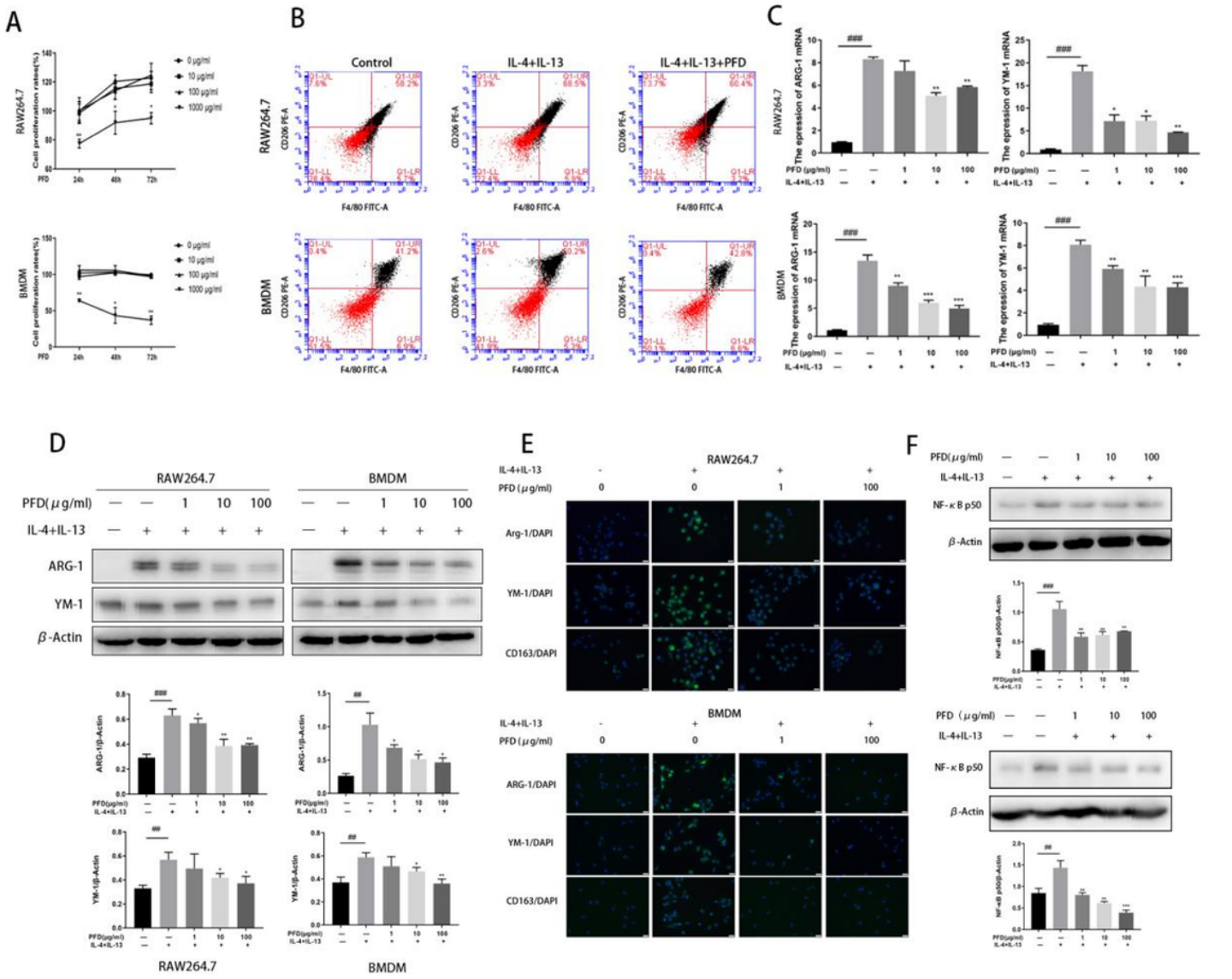

Figure 4

PFD inhibits the polarization of M2 macrophages by downregulating NF-κB p50 expression. (A). Cytotoxic effects of PFD on RAW264.7 cells and BMDMs. Plots showing the effects of different concentrations of PFD on the growth of RAW264.7 cells and BMDMs during the indicated times. The values are the means ±SD, *p<0.05, **p<0.01, when comparing 1000 μg/mL with 0 μg/mL. (B). Flow cytometry was used to analyze the proportion of F4/80+/CD206+ macrophages in the 4 different treatment groups of RAW264.7 cells and BMDMs. (C). qRT-PCR was used to analyze the quantitative mRNA expression of the M2 phenotypic markers ARG-1 and YM-1 in the 4 different treatment groups of RAW264.7 cells and BMDMs. The values are the means ±SD, ##p<0.01 and ###p<0.001, when compared with the untreated group, *p<0.05, **p<0.01, ***p<0.001, when compared with the IL-4 + IL-13-stimulated group. (D). Western blots and associated densitometry analysis of the the protein expression of the M2 phenotypic markers ARG-1 and YM-1 in the 4 different treatment groups of RAW264.7 cells and BMDMs. The values are the means ±SD, ##p<0.01 and ###p<0.001, compared with the untreated group, *p<0.05, **p<0.01, compared with the IL-4 + IL-13-stimulated group. (E). The expression of ARG-1, YM-1 and

CD163 was determined by immunofluorescence staining in 4 different treatment groups of RAW264.7 cells and BMDMs. Scale bar = 20 μm.(F). Western blot and associated densitometry analyses of the expression of NF-κB p50 in the 4 different treatment groups of RAW264.7 cells and BMDMs. The values are the means ±SD, ##p<0.01 and ###p<0.001, compared with the untreated group, *p<0.05, **p<0.01, ***p<0.001, compared with the IL-4 + IL-13-stimulated group.

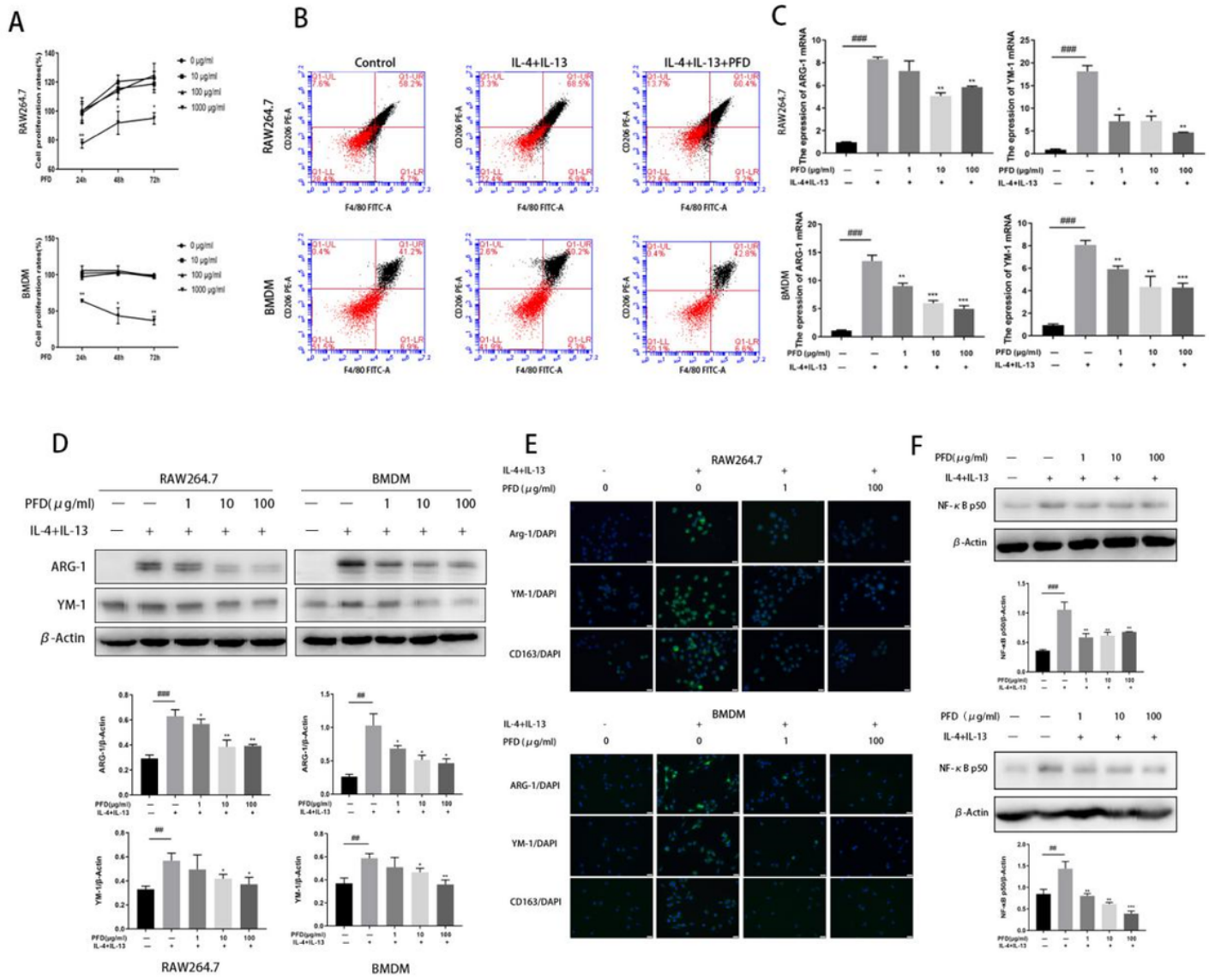

Figure 4

PFD inhibits the polarization of M2 macrophages by downregulating NF-κB p50 expression. (A). Cytotoxic effects of PFD on RAW264.7 cells and BMDMs. Plots showing the effects of different concentrations of PFD on the growth of RAW264.7 cells and BMDMs during the indicated times. The values are the means ±SD, *p<0.05, **p<0.01, when comparing 1000 μg/mL with 0 μg/mL. (B). Flow cytometry was used to analyze the proportion of F4/80+/CD206+ macrophages in the 4 different treatment groups of RAW264.7 cells and BMDMs. (C). qRT-PCR was used to analyze the quantitative mRNA expression of the M2 phenotypic markers ARG-1 and YM-1 in the 4 different treatment groups of RAW264.7 cells and BMDMs. The values are the means ±SD, ##p<0.01 and ###p<0.001, when compared

with the untreated group, *p<0.05, **p<0.01, ***p<0.001, when compared with the IL-4 + IL-13-stimulated group. (D). Western blots and associated densitometry analysis of the the protein expression of the M2 phenotypic markers ARG-1 and YM-1 in the 4 different treatment groups of RAW264.7 cells and BMDMs. The values are the means ±SD, ##p<0.01 and ###p<0.001, compared with the untreated group, *p<0.05, **p<0.01, compared with the IL-4 + IL-13-stimulated group. (E). The expression of ARG-1, YM-1 and CD163 was determined by immunofluorescence staining in 4 different treatment groups of RAW264.7 cells and BMDMs. Scale bar = 20 μm.(F). Western blot and associated densitometry analyses of the expression of NF-κB p50 in the 4 different treatment groups of RAW264.7 cells and BMDMs. The values are the means ±SD, ##p<0.01 and ###p<0.001, compared with the untreated group, *p<0.05, **p<0.01, ***p<0.001, compared with the IL-4 + IL-13-stimulated group.

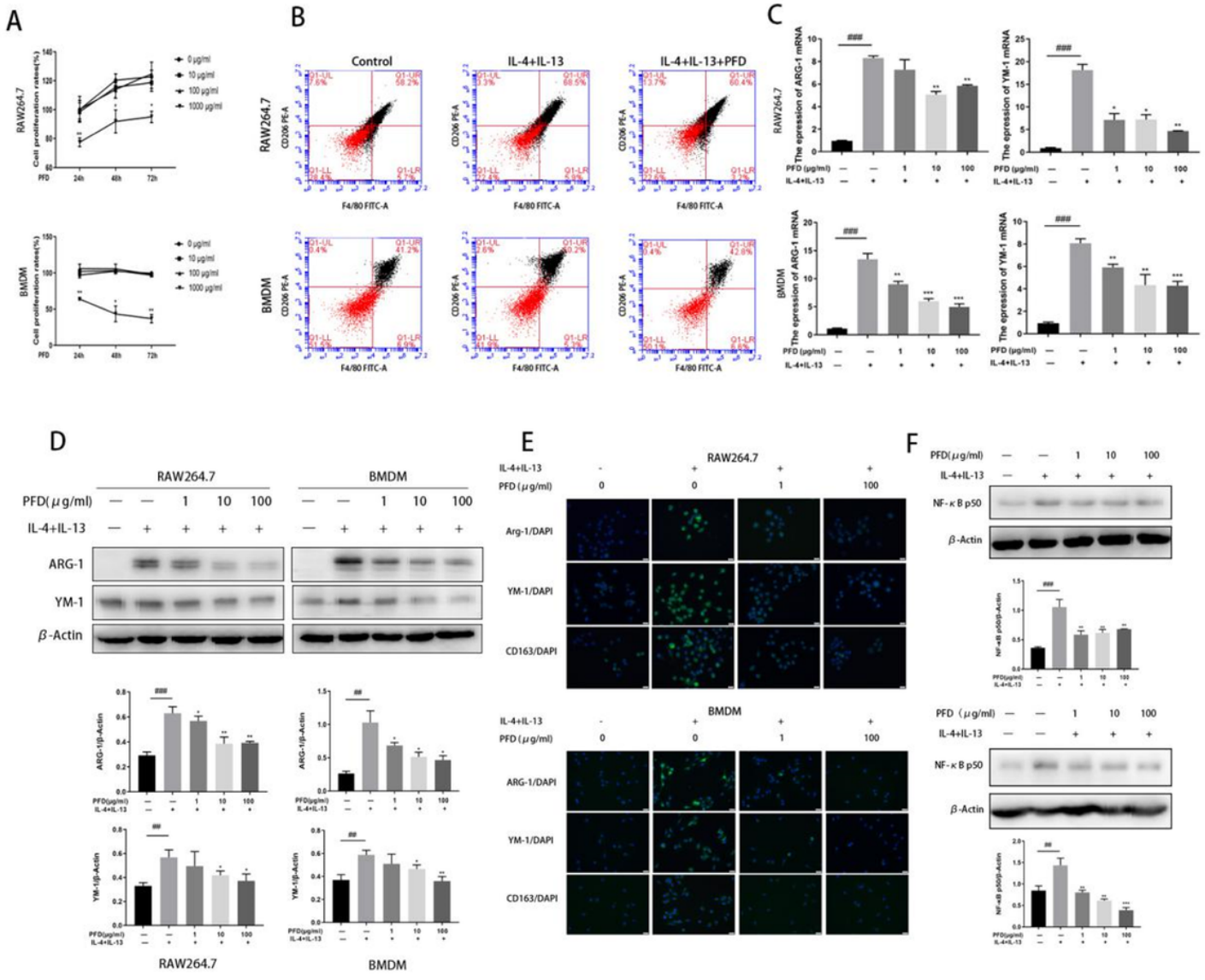

Figure 4

PFD inhibits the polarization of M2 macrophages by downregulating NF-κB p50 expression. (A). Cytotoxic effects of PFD on RAW264.7 cells and BMDMs. Plots showing the effects of different concentrations of PFD on the growth of RAW264.7 cells and BMDMs during the indicated times. The

values are the means ±SD, *p<0.05, **p<0.01, when comparing 1000 μg/mL with 0 μg/mL. (B). Flow cytometry was used to analyze the proportion of F4/80+/CD206+ macrophages in the 4 different treatment groups of RAW264.7 cells and BMDMs. (C). qRT-PCR was used to analyze the quantitative mRNA expression of the M2 phenotypic markers ARG-1 and YM-1 in the 4 different treatment groups of RAW264.7 cells and BMDMs. The values are the means ±SD, ##p<0.01 and ###p<0.001, when compared with the untreated group, *p<0.05, **p<0.01, ***p<0.001, when compared with the IL-4 + IL-13-stimulated group. (D). Western blots and associated densitometry analysis of the the protein expression of the M2 phenotypic markers ARG-1 and YM-1 in the 4 different treatment groups of RAW264.7 cells and BMDMs. The values are the means ±SD, ##p<0.01 and ###p<0.001, compared with the untreated group, *p<0.05, **p<0.01, compared with the IL-4 + IL-13-stimulated group. (E). The expression of ARG-1, YM-1 and CD163 was determined by immunofluorescence staining in 4 different treatment groups of RAW264.7 cells and BMDMs. Scale bar = 20 μm.(F). Western blot and associated densitometry analyses of the expression of NF-κB p50 in the 4 different treatment groups of RAW264.7 cells and BMDMs. The values are the means ±SD, ##p<0.01 and ###p<0.001, compared with the untreated group, *p<0.05, **p<0.01, ***p<0.001, compared with the IL-4 + IL-13-stimulated group.

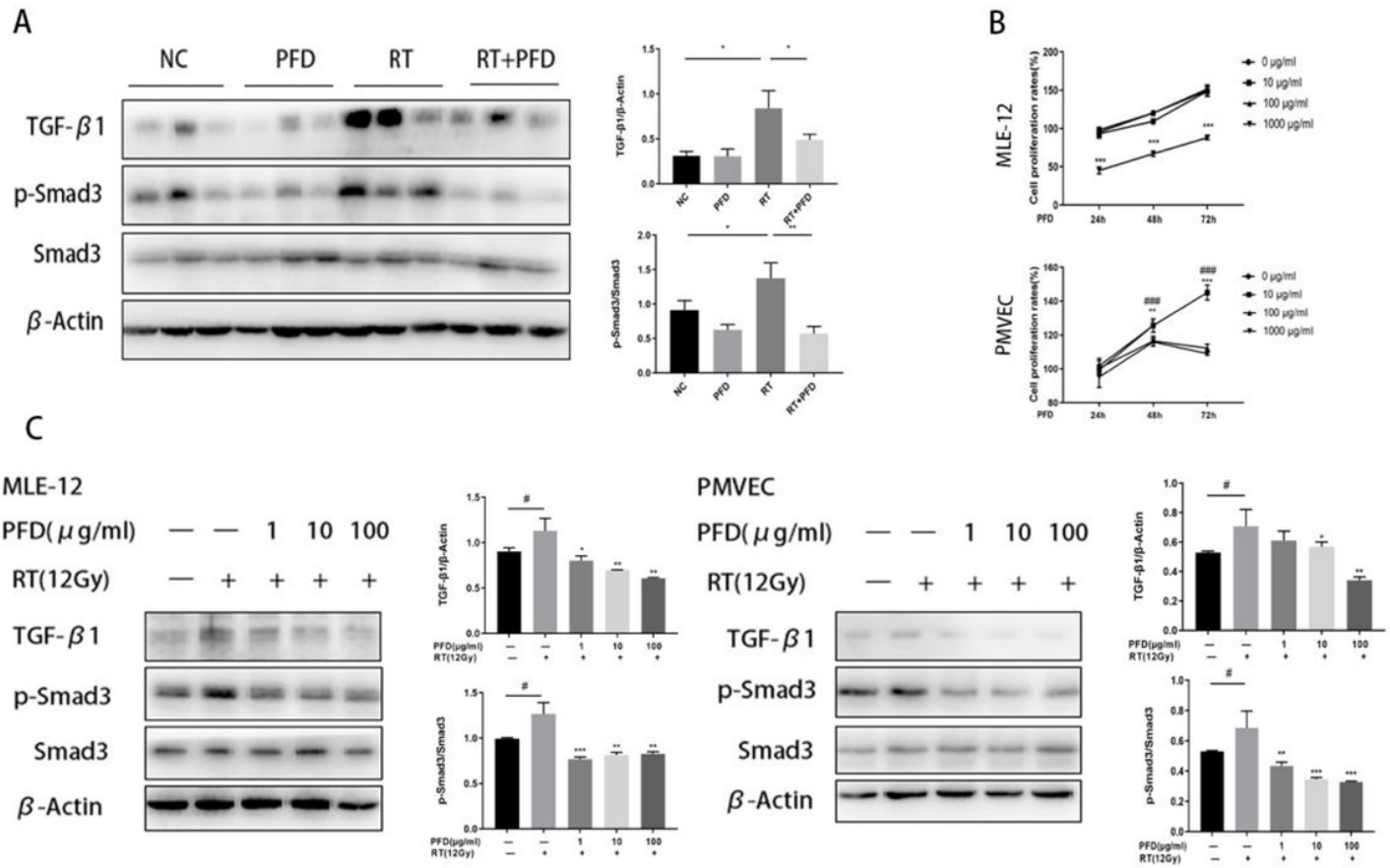

Figure 5

PFD inhibits irradiation-induced activation of the TGF-β1/Smad3 signaling pathway in vivo and in vitro. (A). The expression and quantitative analysis of TGF-β1, p-Smad3, Smad3 and β-actin in lung tissue from

the 4 different treatment groups. N=3; the values are the means±SD,*p<0.05,**p<0.01. (B). Cytotoxic effects of PFD on the proliferation of MLE-12 cells and PMVECs. Plots showing the effects of different concentrations of PFD on the growth of MLE-12 cells and PMVECs over the indicated times. The values are the means±SD. MLE-12 cells: ***p <0.001, 1000 μg/mL compared with 0 μg/mL PMVECs: **p <0.05, ***p<0.001, when comparing 100 μg/mL with 0 μg/mL; ###p<0.001, when comparing 1000 μg/mL with 0 μg/mL. (C) The expression and quantitative analysis of TGF-β1, p-Smad3, Smad3 and β-actin in MLE-12 cells and PMVECs after RT and PFD treatment. The values are the means±SD, #p<0.05, compared with the untreated group, *p<0.05, **p < 0.01, ***p < 0.001, compared with the IL-4 + IL-13-stimulated group.

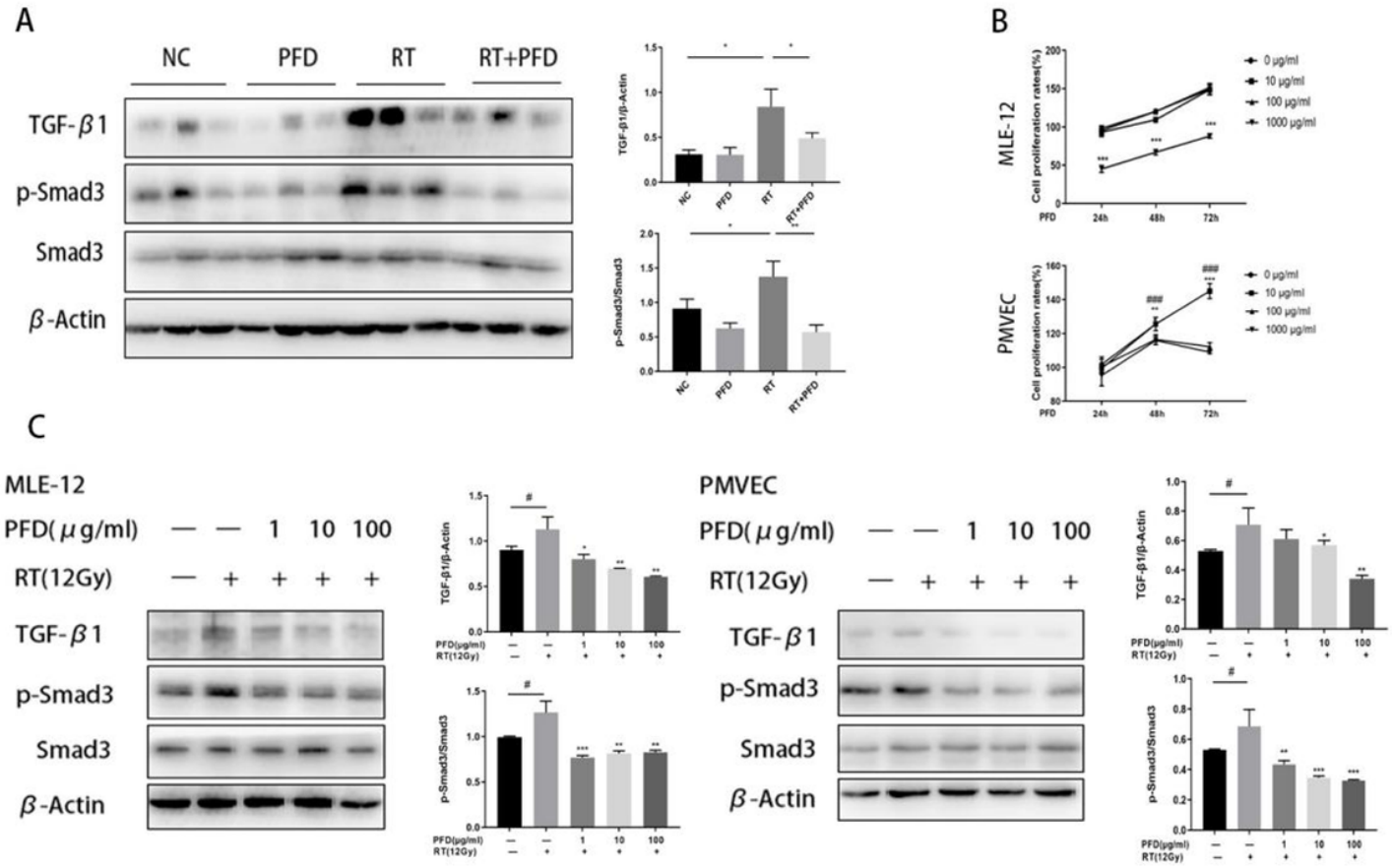

Figure 5

PFD inhibits irradiation-induced activation of the TGF-β1/Smad3 signaling pathway in vivo and in vitro. (A). The expression and quantitative analysis of TGF-β1, p-Smad3, Smad3 and β-actin in lung tissue from the 4 different treatment groups. N=3; the values are the means±SD,*p<0.05,**p<0.01. (B). Cytotoxic effects of PFD on the proliferation of MLE-12 cells and PMVECs. Plots showing the effects of different concentrations of PFD on the growth of MLE-12 cells and PMVECs over the indicated times. The values are the means±SD. MLE-12 cells: ***p <0.001, 1000 μg/mL compared with 0 μg/mL PMVECs: **p <0.05, ***p<0.001, when comparing 100 μg/mL with 0 μg/mL; ###p<0.001, when comparing 1000 μg/mL with 0 μg/mL. (C) The expression and quantitative analysis of TGF-β1, p-Smad3, Smad3 and β-actin in MLE-

12 cells and PMVECs after RT and PFD treatment. The values are the means±SD, #p<0.05, compared with the untreated group, *p<0.05, **p < 0.01, ***p < 0.001, compared with the IL-4 + IL-13-stimulated group.

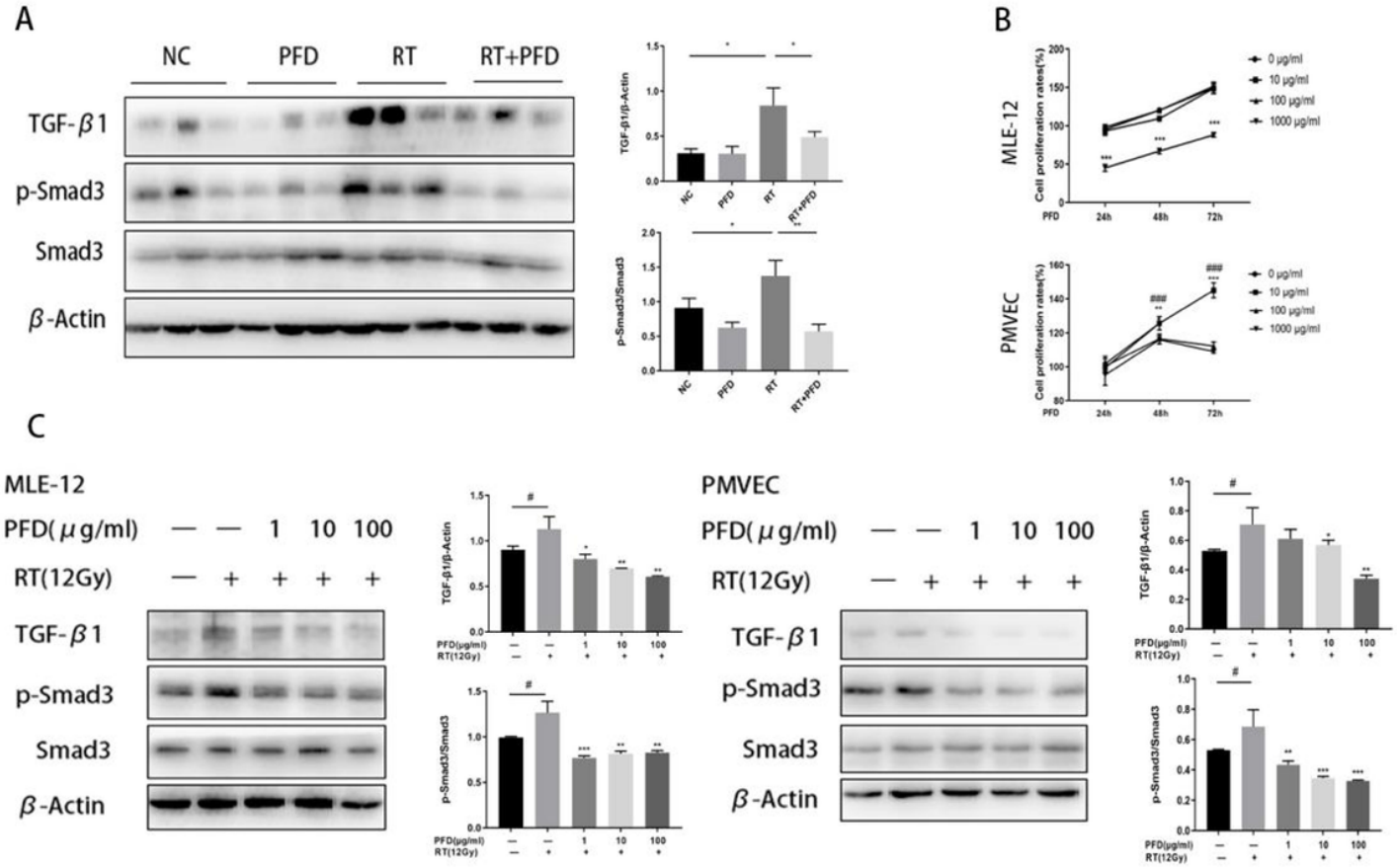

Figure 5

PFD inhibits irradiation-induced activation of the TGF-β1/Smad3 signaling pathway in vivo and in vitro. (A). The expression and quantitative analysis of TGF-β1, p-Smad3, Smad3 and β-actin in lung tissue from the 4 different treatment groups. N=3; the values are the means±SD,*p<0.05,**p<0.01. (B). Cytotoxic effects of PFD on the proliferation of MLE-12 cells and PMVECs. Plots showing the effects of different concentrations of PFD on the growth of MLE-12 cells and PMVECs over the indicated times. The values are the means±SD. MLE-12 cells: ***p <0.001, 1000 μg/mL compared with 0 μg/mL PMVECs: **p <0.05, ***p<0.001, when comparing 100 μg/mL with 0 μg/mL; ###p<0.001, when comparing 1000 μg/mL with 0 μg/mL. (C) The expression and quantitative analysis of TGF-β1, p-Smad3, Smad3 and β-actin in MLE-12 cells and PMVECs after RT and PFD treatment. The values are the means±SD, #p<0.05, compared with the untreated group, *p<0.05, **p < 0.01, ***p < 0.001, compared with the IL-4 + IL-13-stimulated group.

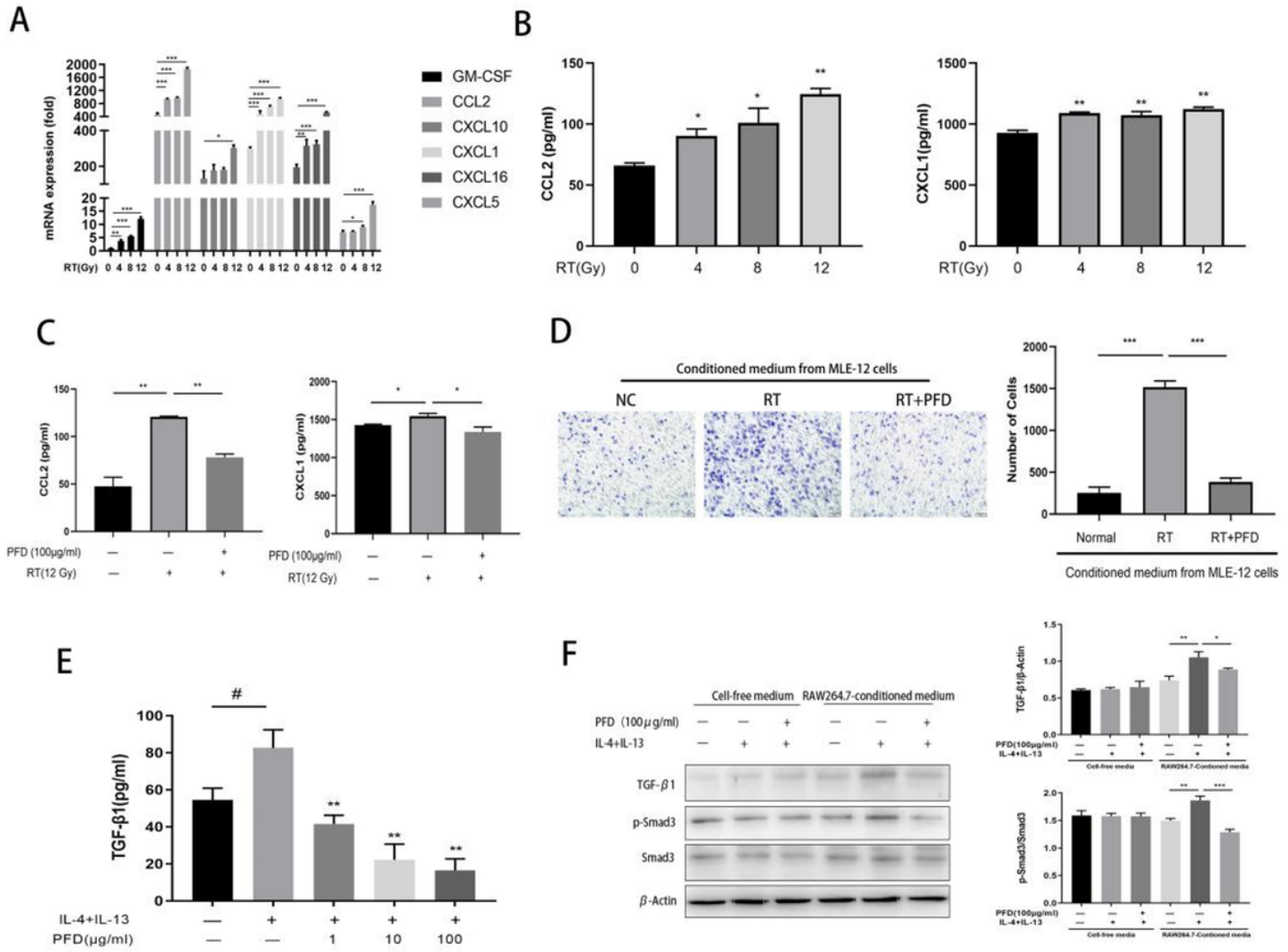

Figure 6

PFD is involved in the crosstalk between alveolar epithelial cells and macrophages. (A). The mRNA expression of GM-CSF, CCL2, CXCL1, CXCL5, CXCL10 and CXCL16 was measured at 24 h after irradiation with 0 to 12 Gy. The values are the means±SD, *p<0.05,**<0.01,***p<0.001 (B). The protein levels of CCL2 and CXCL1 in MLE-12 cell culture supernatants were detected by ELISA after irradiation with 4 different doses. The values are the means±SD, *p<0.05,**<0.01, compared with 0 Gy. (C). The secretion of CCL2 and CXCL1 by MLE-12 cells was measured by ELISA after different treatments with PFD and radiation. The values are the means±SD, *p<0.05,**<0.01. (D). The migration of RAW264.7 cells was assessed in a Transwell assay. Representative images (left) and statistical analysis (right) show the migration of RAW264.7 cells induced by different conditioned media. The values are the means±SD, ***p<0.001.(E). The protein expression of TGF-β1 in culture supernatants of RAW264.7 cells in the groups treated with IL-4+IL-13 and PFD was measured by ELISA. (F). The expression levels of p-Smad3, Smad3 and β-Actin in MLE-12 cells cultured in in conditioned media collected from RAW264.7 cells in the different treatment groups were analyzed by western blotting.

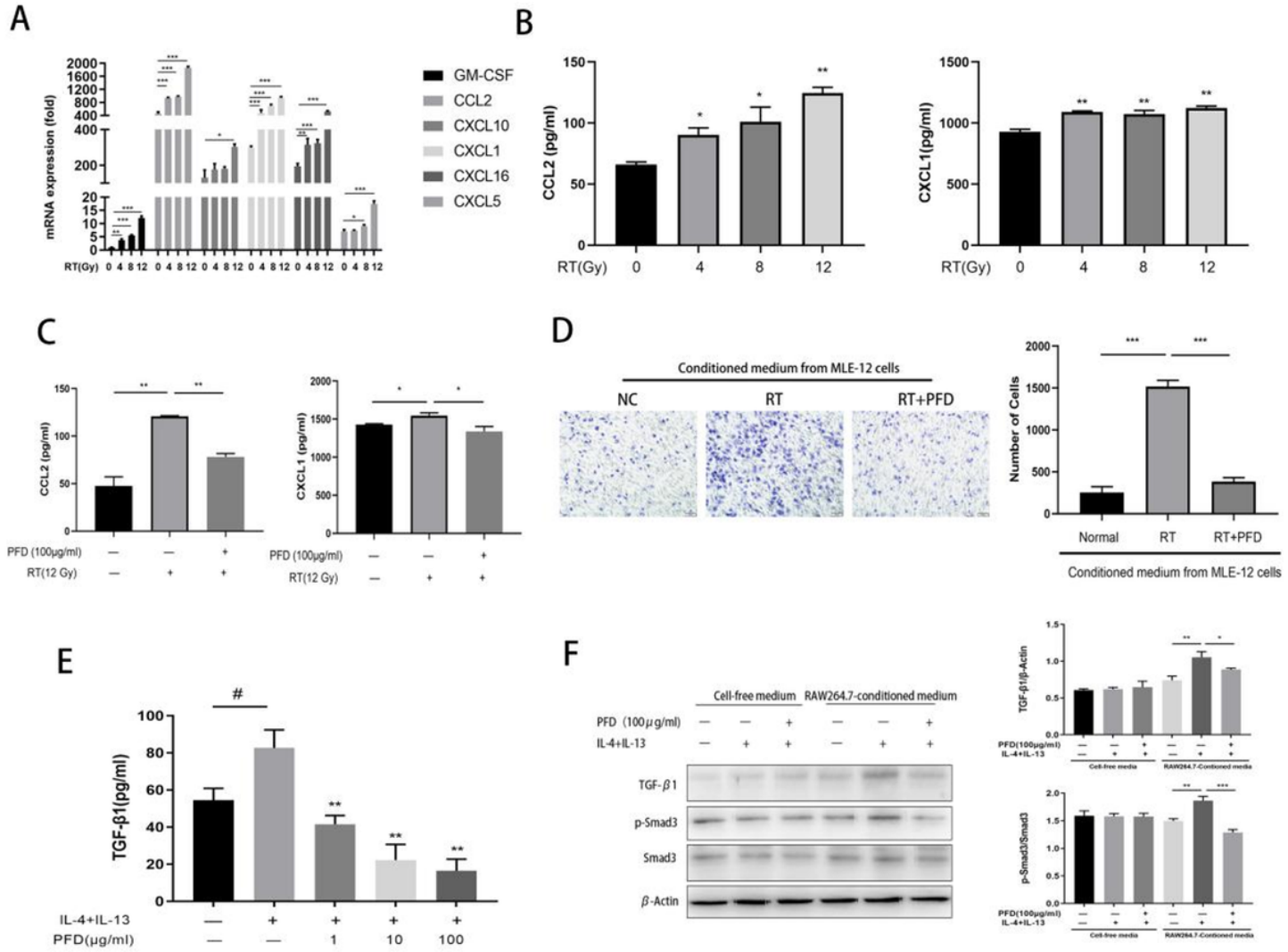

Figure 6

PFD is involved in the crosstalk between alveolar epithelial cells and macrophages. (A). The mRNA expression of GM-CSF, CCL2, CXCL1, CXCL5, CXCL10 and CXCL16 was measured at 24 h after irradiation with 0 to 12 Gy. The values are the means±SD, *p<0.05,**<0.01,***p<0.001 (B). The protein levels of CCL2 and CXCL1 in MLE-12 cell culture supernatants were detected by ELISA after irradiation with 4 different doses. The values are the means±SD, *p<0.05,**<0.01, compared with 0 Gy. (C). The secretion of CCL2 and CXCL1 by MLE-12 cells was measured by ELISA after different treatments with PFD and radiation. The values are the means±SD, *p<0.05,**<0.01. (D). The migration of RAW264.7 cells was assessed in a Transwell assay. Representative images (left) and statistical analysis (right) show the migration of RAW264.7 cells induced by different conditioned media. The values are the means±SD, ***p<0.001.(E). The protein expression of TGF-β1 in culture supernatants of RAW264.7 cells in the groups treated with IL-4+IL-13 and PFD was measured by ELISA. (F). The expression levels of p-Smad3, Smad3 and β-Actin in MLE-12 cells cultured in in conditioned media collected from RAW264.7 cells in the different treatment groups were analyzed by western blotting.

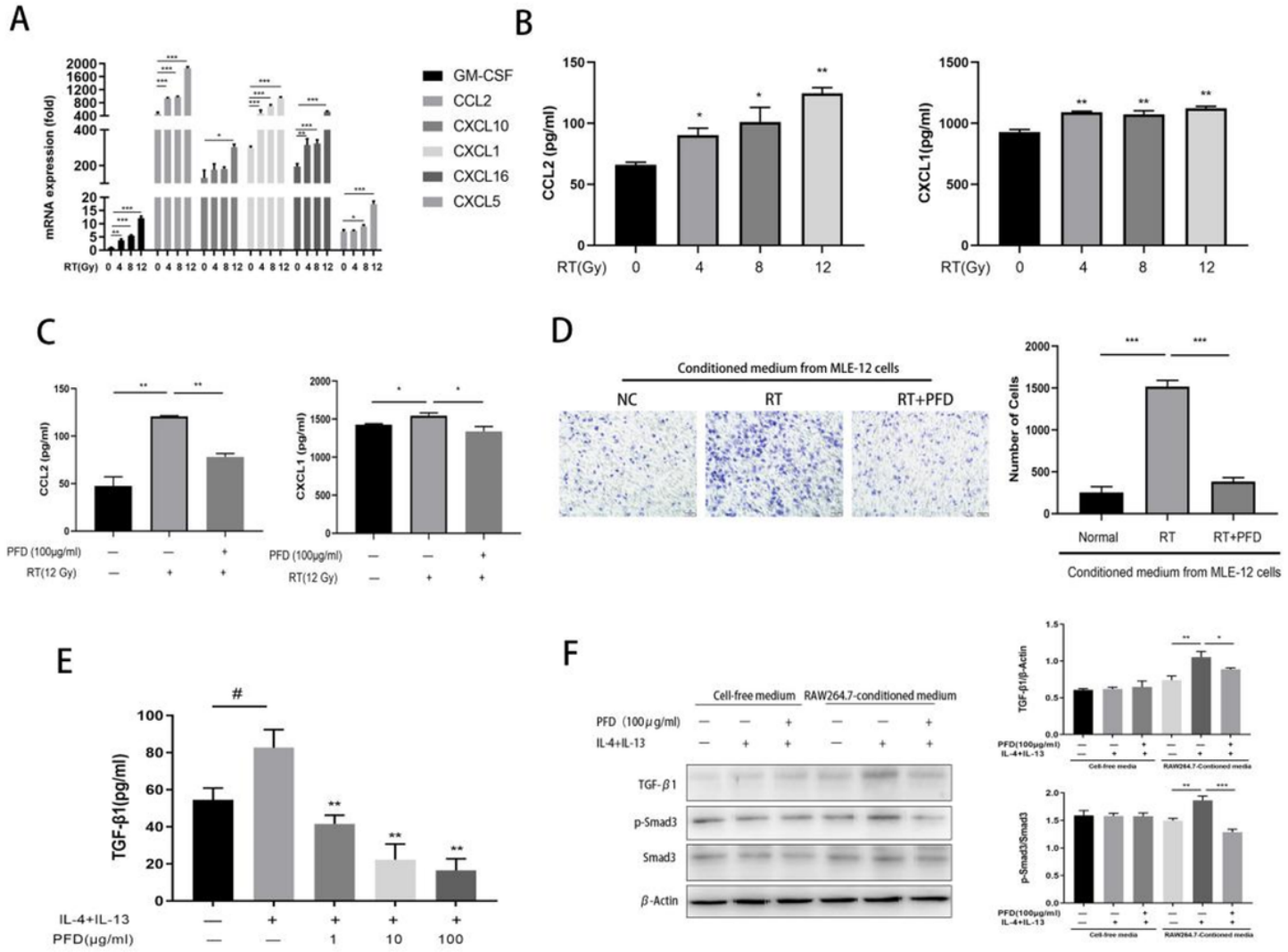

Figure 6

PFD is involved in the crosstalk between alveolar epithelial cells and macrophages. (A). The mRNA expression of GM-CSF, CCL2, CXCL1, CXCL5, CXCL10 and CXCL16 was measured at 24 h after irradiation with 0 to 12 Gy. The values are the means±SD, *p<0.05,**<0.01,***p<0.001 (B). The protein levels of CCL2 and CXCL1 in MLE-12 cell culture supernatants were detected by ELISA after irradiation with 4 different doses. The values are the means±SD, *p<0.05,**<0.01, compared with 0 Gy. (C). The secretion of CCL2 and CXCL1 by MLE-12 cells was measured by ELISA after different treatments with PFD and radiation. The values are the means±SD, *p<0.05,**<0.01. (D). The migration of RAW264.7 cells was assessed in a Transwell assay. Representative images (left) and statistical analysis (right) show the migration of RAW264.7 cells induced by different conditioned media. The values are the means±SD, ***p<0.001.(E). The protein expression of TGF-β1 in culture supernatants of RAW264.7 cells in the groups treated with IL-4+IL-13 and PFD was measured by ELISA. (F). The expression levels of p-Smad3, Smad3 and β-Actin in MLE-12 cells cultured in in conditioned media collected from RAW264.7 cells in the different treatment groups were analyzed by western blotting.

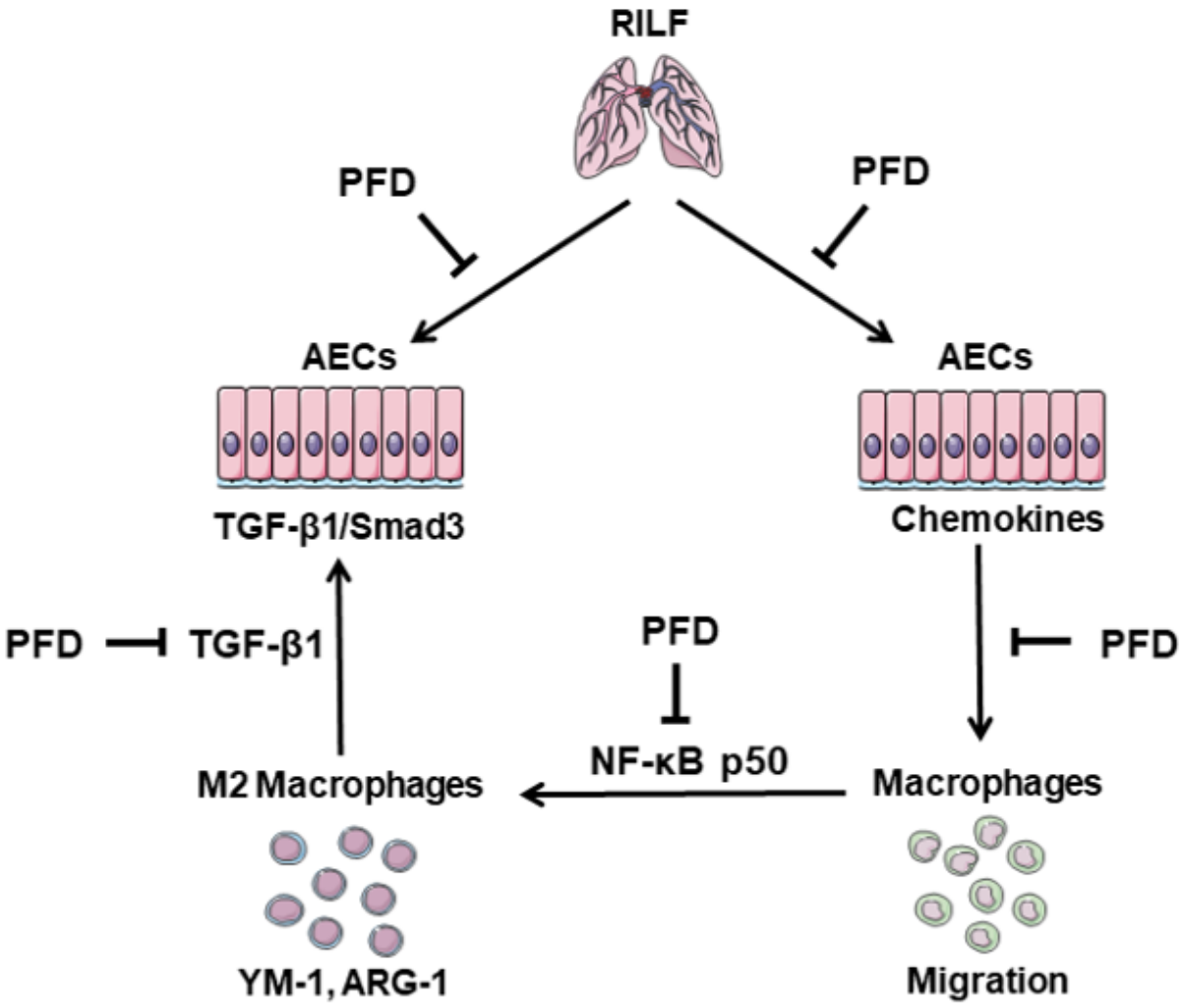

Figure 7

The working model of the preventive and therapeutic effects of PFD on RILF. PFD has a significant inhibitory effect on pulmonary fibrosis and fibrosis in other organs and is a broad-spectrum antifibrosis drug. In our study we show that PFD protects against RILF by reducing the recruitment of M2 macrophages and inhibiting activation of the TGF-β1/Smad3 signaling pathway. PFD is also involved in the crosstalk between macrophages and AECs: 1. PFD reduces the migration of macrophages by inhibiting the secretion of chemokines by MLE-12 cells induced by ionizing radiation. 2. PFD inhibits activation of the TGF-β1/Smad3 signaling pathway in MLE-12 cells by inhibiting the secretion of TGF-β1 by M2 macrophages. Here, we provide a new theoretical basis for the use of PFD in the treatment of RILF. Parts of the figure were drawn using images from Servier Medical Art (https://smart.servier.com/).

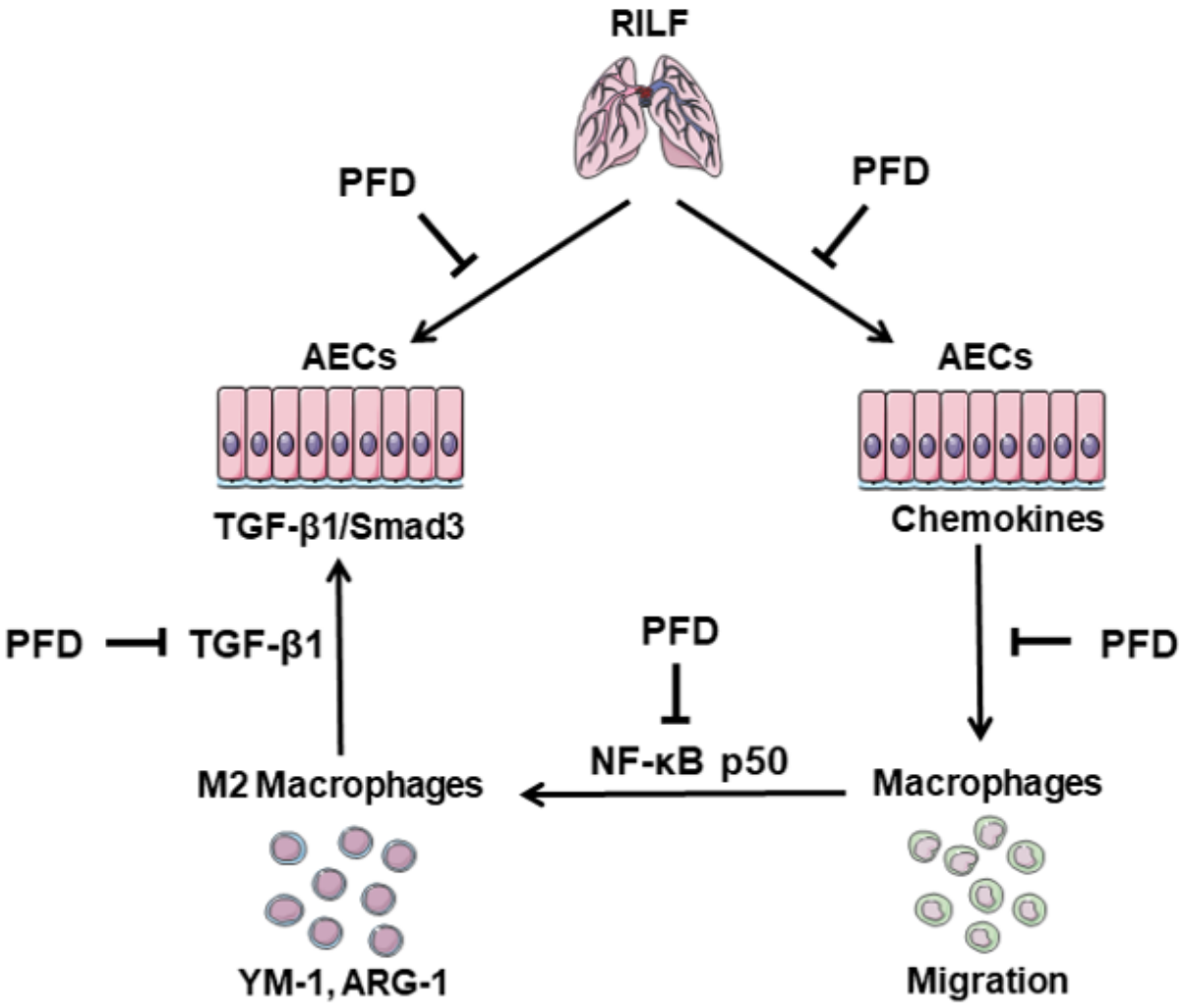

Figure 7

The working model of the preventive and therapeutic effects of PFD on RILF. PFD has a significant inhibitory effect on pulmonary fibrosis and fibrosis in other organs and is a broad-spectrum antifibrosis drug. In our study we show that PFD protects against RILF by reducing the recruitment of M2 macrophages and inhibiting activation of the TGF-β1/Smad3 signaling pathway. PFD is also involved in the crosstalk between macrophages and AECs: 1. PFD reduces the migration of macrophages by inhibiting the secretion of chemokines by MLE-12 cells induced by ionizing radiation. 2. PFD inhibits activation of the TGF-β1/Smad3 signaling pathway in MLE-12 cells by inhibiting the secretion of TGF-β1 by M2 macrophages. Here, we provide a new theoretical basis for the use of PFD in the treatment of RILF. Parts of the figure were drawn using images from Servier Medical Art (https://smart.servier.com/).

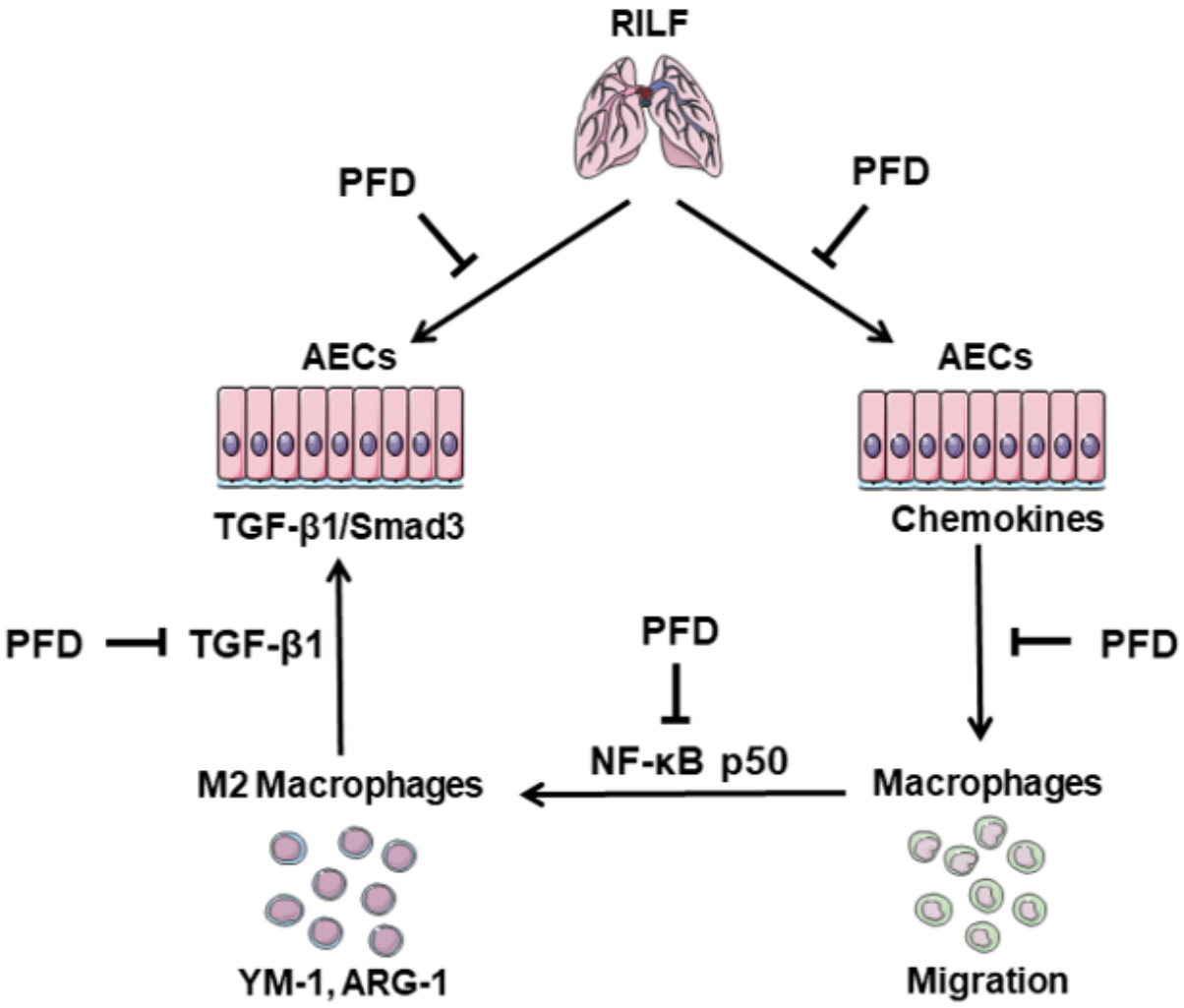

Figure 7

The working model of the preventive and therapeutic effects of PFD on RILF. PFD has a significant inhibitory effect on pulmonary fibrosis and fibrosis in other organs and is a broad-spectrum antifibrosis drug. In our study we show that PFD protects against RILF by reducing the recruitment of M2 macrophages and inhibiting activation of the TGF-β1/Smad3 signaling pathway. PFD is also involved in the crosstalk between macrophages and AECs: 1. PFD reduces the migration of macrophages by inhibiting the secretion of chemokines by MLE-12 cells induced by ionizing radiation. 2. PFD inhibits activation of the TGF-β1/Smad3 signaling pathway in MLE-12 cells by inhibiting the secretion of TGF-β1 by M2 macrophages. Here, we provide a new theoretical basis for the use of PFD in the treatment of RILF. Parts of the figure were drawn using images from Servier Medical Art (https://smart.servier.com/).